Carbon-based flexible electrodes for electrochemical potassium storage devices

Yuhan Wu[1,*], Xiaonan Wu[2], Yinyan Guan[1,*], Yang Xu[3,*], Fa-Nian Shi[1], and Jiyan Liang[1]

[1]School of Chemical & Environmental Engineering, Shenyang University of Technology, Shenyang 110870, China

[2]Department of Chemical Engineering, Hebei Petroleum University of Technology, Chengde 067000, China

[3]Department of Chemistry, University College London, London WC1H 0AJ, UK

*Corresponding authors:

E-mail:

yuhanwu@sut.edu.cn (Yuhan Wu)

guanyinyan@sut.edu.cn (Yinyan Guan)

y.xu.1@ucl.ac.uk (Yang Xu)

Abstract

With the rapid growth of the flexible and wearable electronic market, flexible electrochemical energy storage technologies have made impressive strides. Nonetheless, developing flexible electrodes with low cost, superior safety, and high performance remains a great challenge. In the past few years, potassium-based electrochemical energy storage devices have captured prominent attention by virtue of the cost competitiveness and easy availability of potassium resources. Carbon materials have been widely employed as electrode materials or substrates for flexible energy storage devices due to their excellent properties, such as low weight, non-toxicity, abundance, *etc*. In this review, we summarize the recent advances in carbon materials (e.g. carbon nanofibers, carbon nanotubes, and graphene) for flexible electrochemical potassium storage devices, including potassium-ion batteries, potassium-ion hybrid capacitors, and K-S/Se batteries. Meanwhile, the synthetic strategies of carbon-based flexible electrodes and the achieved electrochemical performance in the reported works are outlined. Finally, challenges to the future development in this field are discussed and perspectives are given.

Keywords: carbon materials, flexible, potassium-ion batteries, potassium-ion hybrid capacitors, K-S/Se batteries

1. Introduction

Since the Sony Company commercialized lithium-ion batteries (LIBs), this kind of electrochemical energy storage technology has rapidly dominated the battery market due to its high efficiency and long-term cycling stability. With continuous development in the following few decades, LIBs have achieved noticeable progress and thus have been widely applied in modern society. In light of the success and advantages of LIBs, researchers gradually pay attention to other lithium-based electrochemical energy storage devices (EESDs) (e.g. Li-ion hybrid capacitors,[1] Li solid-state batteries,[2] Li-S/Se batteries,[3-4] and so on). However, the tricky problem of the shortage (20 ppm in Earth's crust) and uneven distribution (mainly in Latin America) of Li resources largely limits their further development.[5] It is estimated that Li reserves on land will be exhausted around 2080 based on the consumption rate projected for 2050.[6] Therefore, on account of geopolitics and ever-growing price, novel electrochemical energy storage technologies have been explored as alternatives or supplements to lithium-based EESDs.

Recently, considering the similarity of electrochemical storage mechanisms and the advantage in cost, K-based EESDs, such as potassium-ion batteries (PIBs), potassium-ion hybrid capacitors (PIHCs), and K-S/Se batteries, have been developed successively.[7-9] The similar redox potential of K^+/K (−2.93 V *vs*. standard hydrogen electrode [SHE]) to that of Li^+/Li (−3.04 V *vs*. SHE) potentially ensures the comparable energy density of K-based EESDs. K is widely distributed in Earth's crust, and K reserve (17 000 ppm) is about 900 times higher than that of Li.[10] The price of potassium carbonate is much lower than that of lithium carbonate. Also, in contrast to Li, there are no alloying reactions between K and aluminum in the range of low voltages, meaning that cheap and light aluminum foil can be used as both cathode and anode current collectors. Therefore, the production cost will be decreased while the energy density will be increased. Moreover, owing to the low melting point of K (63.5 °C), K metal dendrites would be melted by Joule heat when metallic K growth leads to internal short circuits. The short-circuit would be cut before severe thermal runaway of EESDs, which largely relieves the safety problem caused by metal dendrites.[11] In addition, K-based EESDs exhibit advantages in certain situations. For instance, in propylene carbonate (PC) solution, K^+ has a smaller Stokes radius (3.6 Å), lower desolvation energy (119.2 kJ mol^{-1}), and higher ionic conductivity (15.2 S cm^2 mol^{-1}) compared with Li^+ (**Table 1**), which is in favor of fast diffusion kinetics.[12] Until now, K-based EESDs have

achieved encouraging results and performance. In terms of energy/power densities (calculation based on full cells), PIBs can yield an energy density of >230 Wh kg^{-1} at a power density of 4000 W kg^{-1},[13] while K-chalcogen (S/Se) batteries achieved an energy density of 700 Wh kg^{-1}.[14] As for PIHCs that combine energy densities and power densities, their maximum energy density reaches 152 Wh kg^{-1} at a low power density (350 W kg^{-1}), and an energy density of 112 Wh kg^{-1} could be maintained at a high energy density of 17500 W kg^{-1}.[15] According to the above-mentioned points, K-based EESDs have aroused wide attention and interest.

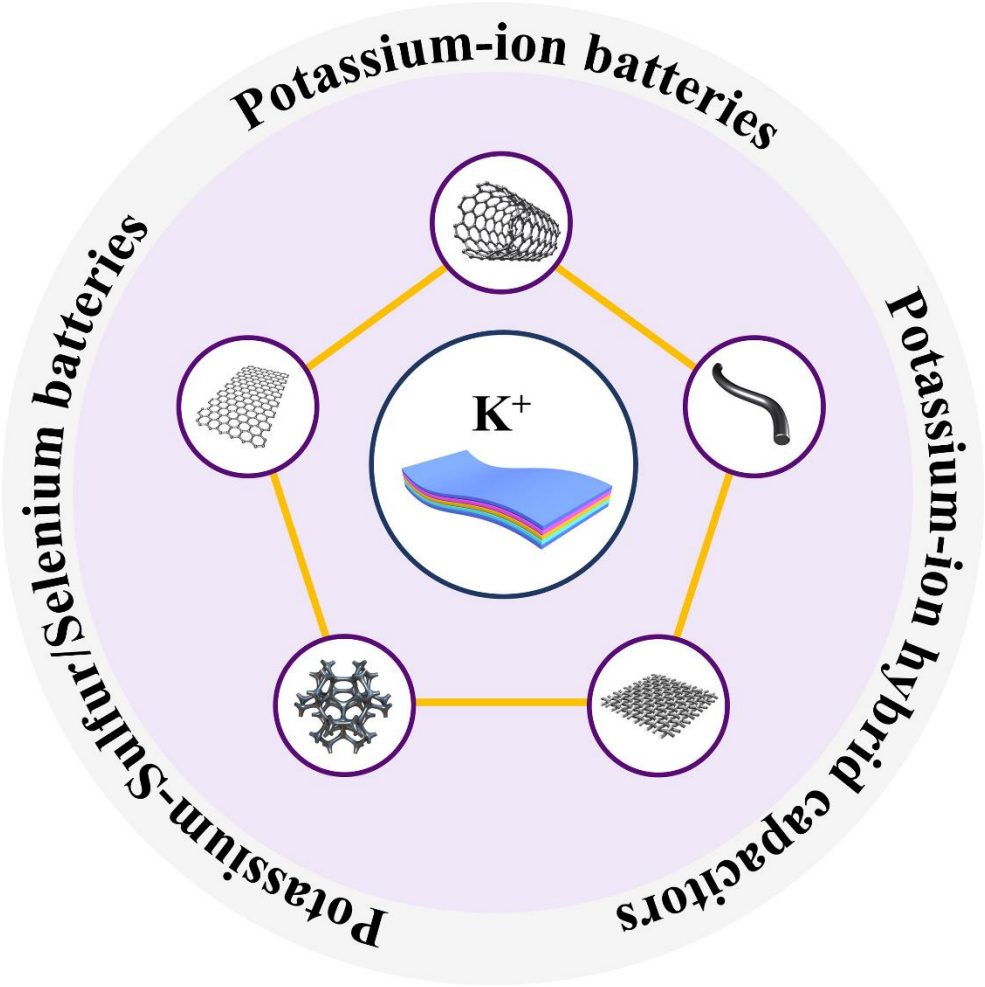

Fig. 1 Typical carbon materials for flexible K-based EESDs

Table 1 Comparison of physical and economic properties between Li and K.[11, 16-17]

	Li	**K**
Atomic number	3	19
Atomic mass (g mol^{-1})	6.94	39.10
Melting point (°C)	180.5	63.5
Abundance in Earth's crust (ppm)	20	17000
Distribution	Mainly in Latin America	Many countries
Alloying reactions with aluminum	Yes	No
Price of carbonate (US $ ton^{-1})	6500	1000
E^0 versus SHE (V)	−3.04	−2.93
Ionic radius (Å)	0.76	1.38
Stokes radius in water (Å)	2.38	1.25
Stokes radius in PC (Å)	4.8	3.6
Ionic conductivity in PC (S cm^2 mol^{-1})	8.3	15.2
Desolvation energy in PC (kJ mol^{-1})	215.8	119.2

Over the past few years, the soaring demand for flexible and wearable electronics, such as bendable smartphones, roll-up displays, and health monitoring skin sensors, has driven great progress in flexible electrochemical energy storage technologies.[18-19] In comparison to conventional EESDs, flexible EESDs have the advantages of foldability, lightweight, and stretchability. With regard to electrode preparation of conventional EESDs (e.g. LIBs), normally, a mixed slurry consisting of active materials, conductive additives, and binders is cast onto foil (copper or aluminum). Herein, insulating and electrochemically inactive binders only play the effect of adhering active materials and conductive additives to current collectors. They not only prevent ions contact active materials but also increase the polarization of electrodes. Conductive additives (e.g. carbon black) are used to maintain good electrical contact between active materials and current collectors; however, their contribution to capacity is very limited. In this case, the presence of these two components has negative effects on volumetric/gravimetric energy densities, and meanwhile, side reactions between electrolytes and them reduce the cycling stability of electrodes. In addition, in conventional EESDs, a metal current collector is used to provide an electron transfer path, but their heavy weight whittle the gravimetric energy density

of full cells down largely.[18] As for flexible EESDs, they have the same principles as conventional EESDs, but, normally, they are binder-, conductive additive-, and current collector-free. The research on flexible EESDs mainly includes developing electrode materials, separators, and electrolytes. To achieve high-performance flexible EESDs with application prospects, it is crucial to develop amenable flexible electrodes. Various materials have been utilized for flexible electrodes, such as carbon materials, metal materials, and polymers.[19] Among them, carbon materials, e.g. graphene, carbon cloth, carbon nanotubes (CNTs), and carbon nanofibers (CNFs), are the most studied due to their merits of high electrical conductivity, superior chemical and thermal stability, low weight, non-toxicity, and large surface areas. These properties play a decisive role in the performance of flexible EESDs.[20-22]

In spite of several reviews on carbon materials for K-based EESDs, their application in flexible K-based EESDs, such a crucial system for electrochemical K storage and flexible electronics, has not been systematically summarized. In this work, the recent progress on carbon materials in flexible K-based EESDs including PIBs, PIHCs, and K-S/Se batteries are summarized by highlighting representative studies (**Fig. 1**). The fabrication method of carbon-based flexible electrodes, the electrochemical storage principle of each K-based EESD, and the achieved electrochemical performance are presented. Furthermore, challenges to the future development in this field are discussed and perspectives are given. We hope our work may provide comprehensive information to promote their further development toward practical application.

2. Fabrication methods

Until now, various technologies have been developed to build carbon-based electrodes for flexible EESDs, such as vacuum filtration,[23-24] electrospinning,[25-26] hydro(solvo)thermal,[27-28] electrodeposition,[29-30] drop-casting,[31] chemical vapor deposition (CVD).[32] These methods are often used in a manner of combination. **Fig. 2** illustrates four main strategies for making carbon-based flexible electrodes, and the detail will be introduced in the following paragraphs.

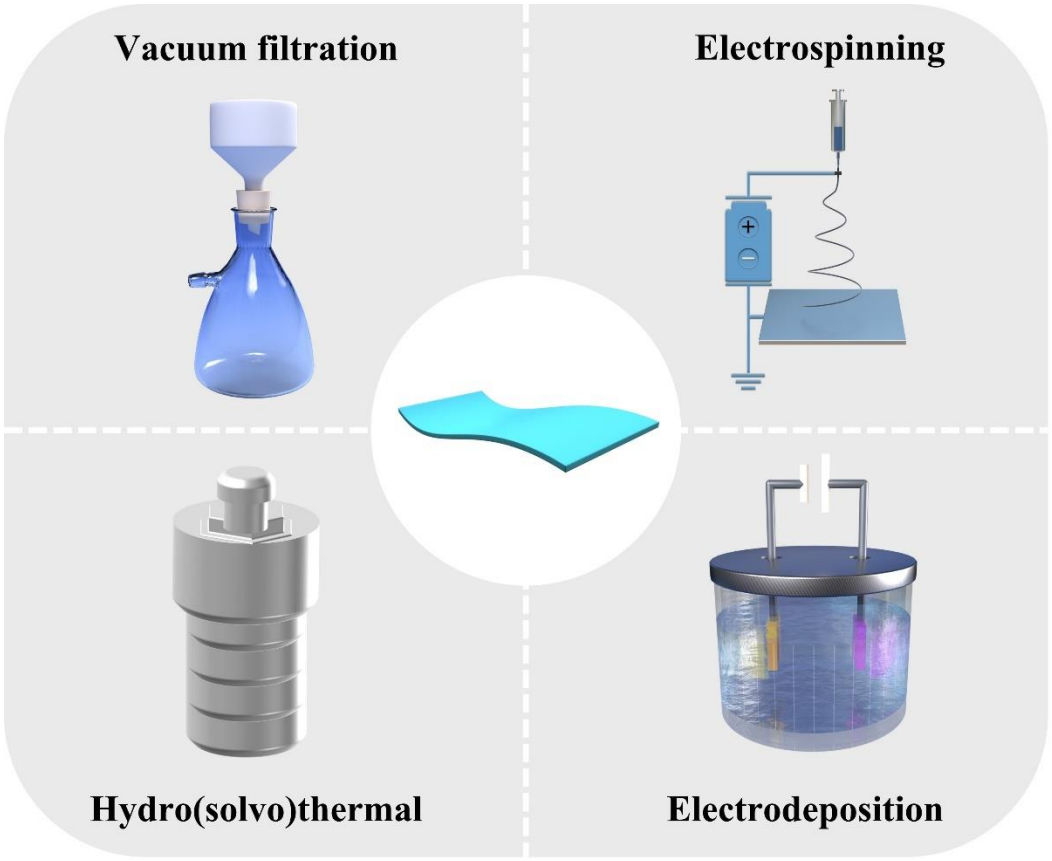

Fig. 2 Typical fabricating methods of carbon-based flexible electrodes.

Vacuum filtration is a simple, scalable, low-cost physical method to make carbon-based flexible electrodes, and has been widely adopted in the reported literature.[23, 33-35] In general, carbon materials (e.g. CNT, graphite, and graphene) and active materials are dispersed into deionized water to form a suspension. Considering the poor dispersion of CNTs in an aqueous solution, CNTs should be modified with acids or surfactants.[23, 33] Thereafter, the suspension is suction filtered by a vacuum filtration setup consisting of a Buchner funnel, a filter membrane, and a vacuum instrument (**Fig. 2**). Finally, the flexible electrode is obtained by drying and peeling off operation.

Electrospinning is a common strategy to fabricate flexible nanofiber films. Typically, active materials or corresponding precursors are homogeneously mixed with a polymer solution, such as polyacrylonitrile (PAN), poly(methylmethacrlate) (PMMA), polyvinyl alcohol (PVA), *etc.*, and then the mixture is electrospun to a film by electrostatic force. The properties of nanofiber films, such as pore structures, electrical conductivity, and mechanical properties, can be adjusted by changing electrospinning progress parameters, polymers, additives, *etc*.[36] To further obtain electrochemically usable carbon-based flexible electrodes, the prepared film should undergo high-temperature

carbonization. Sometimes, a following hydro(solvo)thermal, electrodeposition, gas-phase sulfidation/selenization progress is needed to grow active materials on/in carbon nanofibers.[37-39] It should be noted that some polymers can realize heteroatom doping upon carbonization simultaneously. It is well known that heteroatom doping can enhance the electrochemical reactivity, electronic conductivity, and pseudocapacitance contribution of carbon materials. For example, annealing PAN in an inert atmosphere can obtain N-doping carbon materials directly.

Hydro(solvo)thermal is a commonly used liquid-phase method to synthesize nanomaterials. In the synthesis progress, flexible carbon substrates, such as carbon cloth, graphene papers, and CNF/CNT films are firstly immersed into the precursor solution of active materials. After that, the mixture solution is poured into a sealed steel vessel lined with Teflon, and then, it is heated to a certain temperature for several hours, during which nanomaterials can grow on the surface of carbon substrates. Additionally, to improve the crystallinity of active materials, a subsequent annealing treatment is needed.[40] According to the properties of reaction mediums (e.g. polarity, viscosity, and softness) and heating parameters (e.g. reaction temperatures and time), the morphologies, sizes, phases, and mass loading of active materials can be regulated.[41]

Electrodeposition is a simple strategy for producing coherent active material layers coating carbon-based flexible electrodes by passing current in a solution with a three-electrode system. In the reaction system, flexible carbon substrates as working electrodes are deposited by various materials through electrochemical redox reactions. Electrodeposition can realize fine controllability over deposited materials enabled by varying electrodeposition parameters, including current densities/voltages, solution composition, additives, temperatures, reaction time, *etc*.[42]

Apart from above-mentioned methods, other effective strategies have also been adopted to fabricate carbon-based flexible electrodes. (1) CVD. The CVD method plays two main roles to make flexible carbon-based electrodes. One is used for synthesizing flexible carbon electrodes, such as CNT frameworks and films.[32, 43] The other one is loading active materials onto carbon-based flexible substrates.[44] (2) Pyrolysis. Typically, flexible polymer sponges, papers, *etc*. are used as precursors, and they are annealed at a high temperature under an inert atmosphere to obtain flexible carbon foam and papers.[45] (3) Doctor blade. It is also known as knife coating, being a well-established technique for producing large-area films over rigid or flexible substrates. In a typical procedure, active material-

containing slurry is transferred to a substrate by moving a blade over a flat base.[46] (4) Spray printing. Ink mixed with active materials and carbon materials is printed onto a polymer (e.g. PVA) coating substrate. Later, the polymer is dissolved, and a flexible film is obtained[47] (5) Melt infiltration. This method is mainly used for K-S/Se battery cathodes. Flexible carbon substrates are mixed with bulk S/Se and vacuum-sealed in a quartz tube. Afterward, the tube is heated for several hours to obtain composite cathodes.[48]

Each manufacturing method owns its intrinsic advantages and shortcoming. Vacuum filtration is a feasible method for industrially large-scale production because only mechanical stress is required when construct carbon-based flexible electrodes. This method can realize the precise and simple regulation of the composition of flexible electrodes by changing the amount of added materials. However, the interaction between carbon materials and active materials is weak, which is negative on the stability of flexible electrodes during electrochemical cycling. Electrospinning is a high-efficient and widely applicable technology to fabricate flexible 2D fibric films. After carbonization treatment, the electrospun film transfers into flexible CNF films or active material-CNF composite films. The flexible CNF film can be further served as a flexible substrate to plant active materials by hydro(solvo)thermal, CVD, electrodeposition, *etc*, while flexible active material-CNF composite films can be applied directly. However, the high temperature used in carbonization greatly increases the production cost. In addition, some kinds of embedded active materials are not stable at high temperatures, leading to their decomposition or phase transfer. Hydro(solvo)thermal is a good route to grow active materials onto flexible carbon substrates and meanwhile, can realize the nanostructuring of active materials. It is well-known that nanostructured active materials have large specific surface areas and short ion and electron diffusion length. However, its reaction conditions and processes are harsh and time-consuming, and it is difficult for large-scale applications. Also, the volume expansion of active materials during potassiation cannot be solved because they are exposed on the surface of carbon substrates. This problem also persecutes the composite electrode prepared by electrodeposition and CVD methods. In addition, as for electrodeposition and CVD, the high cost and strict synthesis conditions severely limit their practical applications. Moreover, many materials cannot be deposited by these two methods. Accordingly, none of them is perfect; the cost, electrochemical performance, material property, application environment, *etc*. should be considered and balanced in advance.

3. Application in flexible electrochemical potassium storage devices

3.1. PIBs

3.1.1. Potassium storage mechanisms

Similar to LIBs, PIBs have a typical sandwich configuration, consisting of an anode, a cathode, a porous membrane, and an appropriate electrolyte. During charging, K^+ is extracted from cathodes and impregnated into K salt-containing electrolytes immediately. Meanwhile, the K^+ of electrolytes is inserted into anodes. Upon discharging, a reverse process takes place. Owing to the whole discharge-charge reaction process being similar to a rocking chair, this kind of battery system is named "rocking-chair batteries".[11]

3.1.2. CNF-based flexible electrodes

For flexible electrodes, CNFs are a common flexible material as active materials or substrates, and the combination of electrospinning and carbonization is the most widely adopted method to fabricate CNF films. The entire surface of such 2D films can contact electrolytes, and 1D nanofibers with high conductivity are favorable to the transportation of electrons. Normally, the prepared CNF film has good flexibility and thus can be used directly as flexible electrodes. Xu *et al*. utilized PAN as a precursor to synthesize a porous carbon nanofiber paper by electrospinning combined following carbonization and explored its electrochemical potassium storage capability.[49] The porous CNF paper exhibited good flexibility, and there was no fracture after bending 180 degrees. The porous structure could mitigate the volume expansion during K^+ insertion effectively; the radius expansion of CNFs is negligible (~0.7%) after full potassiation. Serving as a PIB anode, it showed a high reversible capacity of 270 mA h g^{-1} at 0.02 A g^{-1} and a very low decay rate of 0.01% per cycle over 1200 cycles. After an electrochemical cycling test, the porous CNFs remained a well-interconnected entire architecture without fracture or pulverization. Like other carbon materials, morphologies also have a great impact on the electrochemical properties and behaviors of CNFs. Zheng and co-workers constructed multichannel CNFs by regulating the ratio of PMMA/PAN.[50] The fibers without adding PMMA showed the typical smooth surface of PAN-derived CNFs, while the multichannel morphologies gradually formed and became obviously with increasing the amount of PMMA (**Fig. 3a**). However, the excessive PMMA led to the split of CNFs, thus reducing the mechanical property. As a flexible electrode, this is not conducive to practical applications. Electrochemical tests showed that the material with the optimized ratio as

anodes possessed superior cycling stability (110.9 mA h g^{-1} at 2000 mA g^{-1} after 2000 cycles) and rate performance. Such high performance was attributed to plentiful space for volume changing, highly conductive interconnected structures for fast electrons and K^+ transfer, and *in situ* N-, O-doping provided more active sites for K^+ storage. Template methods are another good option for controlling the morphology of CNFs prepared by electrospinning. Guo's group took ZnO as a template to design necklace-like N-doped hollow carbon possessing hierarchical pores.[51] Monodisperse ZnO nanospheres were firstly mixed with PAN and dimethylformamide to form an electrospinning precursor, and then it was electrospun to a fiber film. In the following successive high-temperature treatment under NH_3 and Ar, ZnO was removed, while necklace-like hollow carbon fibers were obtained (**Fig. 3b**). The ultra-high pyridinic/pyrrolic-N doping, large specific surface area, and porosity could facilitate the (de)intercalation of K^+ significantly. Combining these merits, it delivered a high capacity of 293.5 mA h g^{-1} at a current density of 100 mA g^{-1} and showed excellent rate capability of 204.8 mA h g^{-1} at 2000 mA g^{-1} and cycling life (161.3 mA h g^{-1} at 1000 mA g^{-1} after 1600 cycles) when it was served as an anode.

Electrospun CNFs are also used as a matrix for conversion- and alloying-type materials to alleviate their problem of volume expansion during potassiation. Meanwhile, flexible composite electrodes with high capacities can be obtained. Metal chalcogenides (MCs) are also promising research objects by virtue of their high theoretical specific capacities and unique morphologies. [52-53] In general, there are two composite types. One is embedding MCs into CNFs, where CNFs can improve the electronic conductivity of MCs and inhibit the large volume expansion of MCs during conversion/alloying reactions. Firstly, MCs or MC precursors are dispersed into an electrospinning precursor uniformly. Thereafter, the mixing solution is electrospun to a film. Finally, the MC-embedded CNF film is obtained through carbonization or sulfidation/selenization. For example, Ci *et al*. reported freestanding and flexible SnS_2@C nanofibers as a foldable PIB anode by a combination preparation process of electrospinning, pyrolysis, and sulfidation.[26] The SnS_2@C nanofiber film displayed superior flexibility in deformation tests (**Fig. 3c**). The K^+ storage capability was firstly evaluated in half cells. Its capacity remained 342.8 mA h g^{-1} (at 100 mA g^{-1}) after 200 cycles, corresponding to a 96.62% capacity retention ratio. Also, the rate capacity could reach 219.4 mA h g^{-1} at 5000 mA g^{-1}, and a capacity of 183.1 mA g^{-1} was sustained after 1000 cycles in a long-term cycling test at 2000 mA g^{-1}. Considering its good

flexibility, a pouch-packed full cell was assembled. As shown in **Fig. 3d**, the pouch cell could light 27 red LEDs on easily, and kept working in folded and subsequently released states. The other one is coating MCs onto the surface of CNFs. During preparation processes, electrospun polymer fiber films are firstly carbonized, and then the obtained carbon fiber film is subjected to CVD, electrodeposition, or hydro(solvo)thermal treatment to plant MC nanosheets. This method is generally adopted by layered MCs because the agglomeration problem of MC nanosheets can be suppressed, thus exposing more active sites. Huang *et al*. developed a dual anionic vacancy-rich MoSSe array anchored carbon nanofibers membrane (v-MoSSe@CM) as a free-standing anode for PIBs **(Fig. 3e)**.[37] PAN nanofiber membrane was obtained by electrospinning, and then it was pre-oxidized and carbonized under an inert atmosphere. Afterward, v-MoSSe arrays were anchored through hydrothermal and annealing processes. The composite maintained K storage capacities of 234.2 and 220.5 mA h g^{-1} at 0.5 A g^{-1} after 200 and 1000 cycles, respectively. A rate performance test featured a high capacity of 202.6 mA h g^{-1}@5 A g^{-1}.

Alloying-based metal materials, such as Sb, Bi, and Sn, have been investigated as electrode materials because they can offer high theoretical capacities. However, they usually undergo a huge volume change during cycling processes, and thus electrodes may suffer from mechanical stress, delamination, and pulverization. These problems are normally the origin of high voltage hysteresis and poor cycling performance.[54-55] As mentioned before, electrospinning can encapsulate active materials within carbon fibers, which can largely relieve the volume expansion of alloying-based metals. For instance, Zhou's group impregnated ultrafine Sb nanocrystals within nanochannel-containing CNFs.[56] The ultrasmall Sb nanocrystals and the hollow nanochannels enabled fast reaction kinetics and easy strain relaxation. Exactly due to these advantages, the electrode as the anode of PIBs achieved a high capacity and good cycling stability (225 mA h g^{-1} at 1 A g^{-1} after 2000 cycles) (**Fig. 3f**). Apart from MCs and alloying-based materials, metal oxides, metal phosphides, *etc*. were also used in flexible PIB electrodes and exhibited great prospects.[57-59]

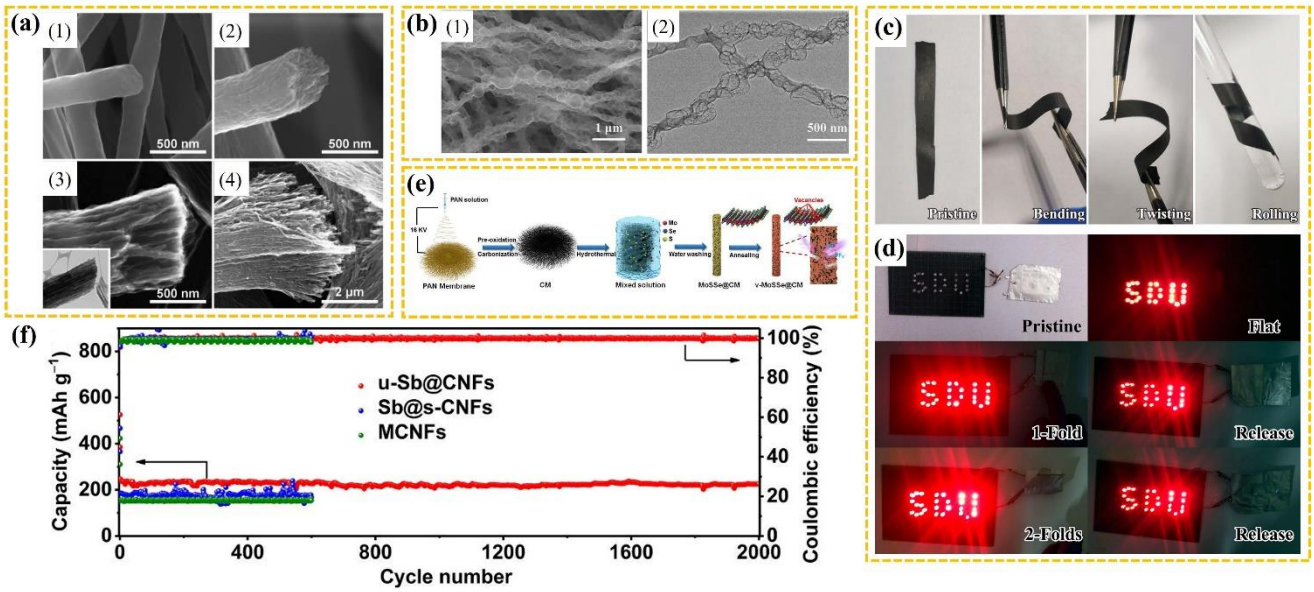

Fig. 3 (a) SEM images of prepared MCCFs with PMMA to PAN ratio of (1) 0, (2) 1, (3) 2, (4) 3.[50] (Reprinted with permission, Copyright 2019, Wiley). (b) (1−2) SEM and TEM images of necklace-like N-doped hollow carbon.[51] (Reprinted with permission, Copyright 2019, The Royal Society of Chemistry). (c) Demonstration of the flexibility of SnS_2@C-2 nanofibers. (d) Demonstrations by lighting LEDs at different mechanical states.[26] (Reprinted with permission, Copyright 2021, The Royal Society of Chemistry). (e) Schematic illustration of the preparation of v-MoSSe@CM.[37] (Reprinted with permission, Copyright 2019, Wiley). (f) Prolonged cycling performance of u-Sb@CNFs, Sb@s-CNFs, and MCNFs at 1 A g^{-1}.[56] (Reprinted with permission, Copyright 2020, Elsevier).

3.1.3. CNT-based flexible electrodes

CNTs have two types, i.e. single-walled CNTs (SWCNTs, single graphene sheet) and multi-walled CNTs (MWCNTs, additional graphene sheets rolled up around SWCNTs with *van der Waals* force between neighboring layers). 1D electron transport path ensures their high electrical conductivity. Additionally, they have high tensile strength and chemical resistance. CNTs have been widely used as electrode materials or act as carbon modification materials.[60] The most common and facile method to construct CNT-based flexible electrodes is vacuum filtration. For instance, Xu and co-workers designed a $K_{0.5}V_2O_5$ and CNTs hybrid film through vacuum filtration and investigated its electrochemical properties as a PIB cathode.[61] Evaluating in PIB half cells, the $K_{0.5}V_2O_5$/CNT electrode exhibited good reversible specific capacities, retention, and rate performance. It was coupled with a hard carbon anode to assemble a flexible cable-shaped PIB full cell (**Fig. 4a**). The full cell could deliver a capacity of 51

mA h g^{-1} at 20 mA g^{-1} after 30 cycles and could power a red LED at various bending angles. Recently, a CVD combing two-step solvothermal strategy was adopted to fabricate metallic octahedral $CoSe_2$ threaded by an N-doped MWCNT framework (NCNF@CS) (**Fig. 4b)**.[43] NCNF was first synthesized by CVD, and then CoO_x and $CoSe_2$ were formed on NCNF successively through solvothermal. In flexible testing, NCNF@CS displayed high flexibility (**Fig. 4c**). When it was employed as a PIB anode, a capacity of 253 mA h g^{-1} at 0.2 A g^{-1} after 100 cycles with ~85.3% capacitance retention was achieved, and a long-term cycling test featured a stable capacity (173 mA h g^{-1} at 2.0 A g^{-1} after 600 cycles).

3.1.4. Graphene-based flexible electrodes

Graphene, a 2D sheet, is comprised of sp^2-bonded single-layer carbon atoms with a honeycomb lattice structure. It has high electron mobility (>15000 cm^2 V^{-1} at room temperatures), low resistivity (even lower than that of silver), and a high surface area (~2630 m^2 g^{-1}).[62-64] All of these excellent properties have aroused extensive attention in electrochemical energy storage. In graphene, every atom is available, leading to high electrochemical activity and low diffusion resistance for ions to access the surface.[65] It is calculated that its theoretical specific capacity is 744 mA h g^{-1}.[66] Moreover, the merits of exceptional mechanical robustness, good flexibility, and ultralow weight make graphene become a promising candidate for flexible electrodes. The flexible graphene film/paper can be used as an electrode and a substrate to form a hybrid electrode.

Zhang *et al*. fabricated a free-standing film of potassium titanate (KTO)/rGO with a sandwiched structure through a strategy of the confined transformation of MXene/rGO hybrid films.[35] The film could display outstanding electrochemical performance in both cycling and rate tests when it was applied as a PIB anode. This was attributed to the synergetic effect of the unique sandwiched structure, short diffusion distance originating from ultrathin KTO layers, enhanced electronic conductivity provided by graphene, and good compatibility between layered nanosheets. Likewise, to achieve high-performance electrode materials, graphene has been hybridized with other active materials to form composite electrodes. Considering the issues of large volume variation, poor intrinsic electronic, and ionic conductivity of transition-metal phosphides, hollow FeP nanospheres were encapsulated within a 3D graphene framework (3DG/FeP) to form a flexible and hierarchically porous PIB anode (**Fig. 4d)**.[67] The porosity and high mechanical strength endowed 3DG/FeP aerogel with good flexibility, as shown in **Fig. 4e**. In comparison to those of pure FeP, the rate and cycling performance of 3DG/FeP had

significant improvement. Also, 3DG/FeP displayed ultrahigh cycling stability with capacity retention of 97.6% at 2 A g^{-1} after 2000 cycles. Qiu *et al*. reported a bismuth nanosheet/graphene (BiNS/rGO) electrode prepared by vacuum filtration (**Fig. 4f**).[68] Bi as an alloy-based electrode material has a high theoretical specific capacity, but it endures a large volume expansion of ~411% during discharge processes, resulting in severe capacity fading. BiNS/rGO network with controlled pore structures which effectively tackle the expansion and alleviate the structural failure of electrodes during electrochemical cycling, and facilitate the transfer of K^+ and electrons. When cycled at 0.5 A g^{-1}, the BiNS anode only kept a reversible capacity of 104 mA h g^{-1} after 90 cycles, while BiNS/rGO still delivered 272 mA h g^{-1} after the same cycling number. As for rate performance, the capacity of BiNS was only 30 mA h g^{-1} at 2 A g^{-1}, and there was nearly no capacity when current densities were higher than 5 A g^{-1}. By contrast, the capacity of BiNS/rGO maintained 100 mA h g^{-1} even at 10 A g^{-1}.

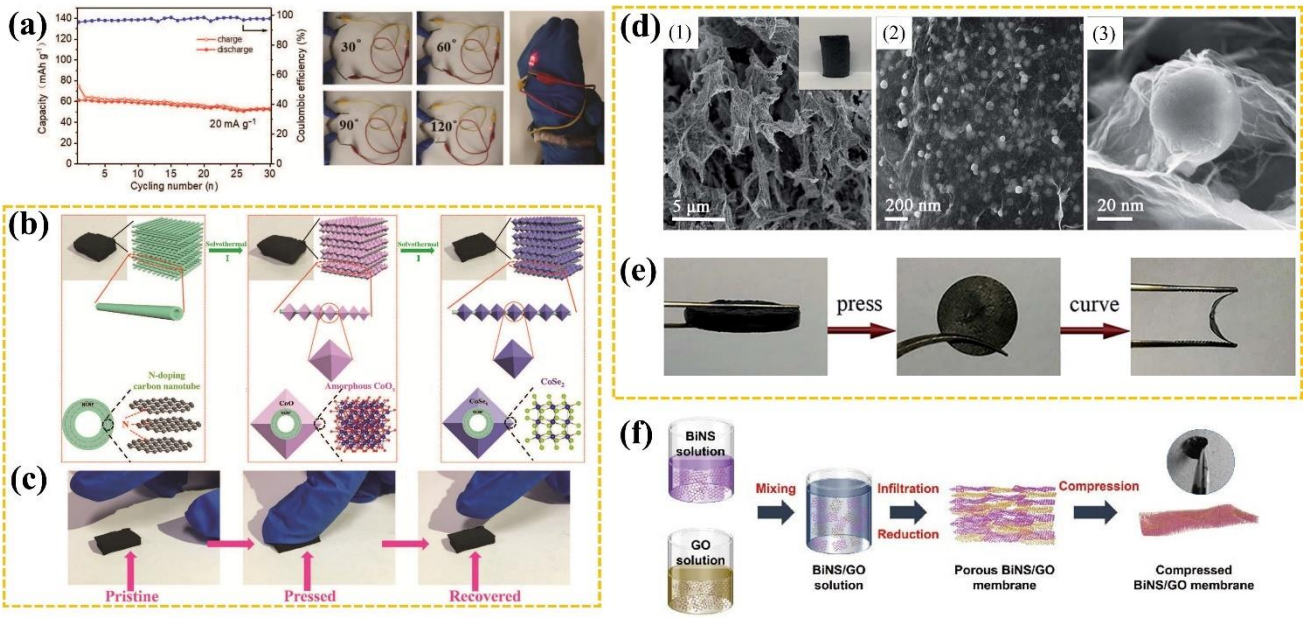

Fig. 4 (a) Cycling stability at a current density of 20 mA g^{-1} of the cable-shaped PIB and photographs of a red LED powered by the cable-shaped PIB at various bending angles.[61] (Reprinted with permission, Copyright 2021, The Royal Society of Chemistry). (b) Schematic illustration of the preparation of NCNF@CS. (c) Optical images of flexibility test using NCNF@CS-6 h.[43] (Reprinted with permission, Copyright 2018, Wiley). (d) (1−3) SEM and images of 3DG/FeP. (e) Flexible 3DG/FeP film electrode.[67] (Reprinted with permission, Copyright 2020, The Royal Society of Chemistry). (f) Schematic illustration of the fabrication of the relatively dense BiNS/rGO mambrane.[68] (Reprinted with permission, Copyright 2020, Springer-Verlag).

3.1.5. Carbon sponge/carbon foam/carbon cloth-based flexible electrodes

Carbon sponges, carbon foam, and carbon cloth, such carbon materials with high flexibility, are commonly used to synthesize flexible electrodes owing to their great electrical conductivity, superior mechanical strength, and large surface areas to accommodate active materials. In addition, they are scalable and commercially available. Qiu *et al*. developed a nitrogen and phosphorus dual-doped vertical graphene (N, P-VG) uniformly grown on carbon cloth (N, P-VG@CC) as the binder-free anode of flexible PIBs (**Fig. 5a**).[13] The self-supported VG nanosheet arrays were firstly planted on carbon cloth using a microwave plasma-enhanced CVD method. Afterward, it was annealed in NH_3 mixed with PH_3 generated by the decomposition of $NaH_2PO_2 \cdot H_2O$ to realize N and P co-doping simultaneously. Electrochemical tests in half cells showed that N, P-VG@CC had superior cycling and rate performance. Moreover, a flexible full cell was assembled using Prussian blue (KPB) as the cathode. As a result, the full cell delivered a reversible capacity of 116.25 mA h g^{-1} at 50 mA g^{-1} and only had a 14.1% capacity decay after 150 cycles. The maximum energy density and power density were able to reach 232.5 W h kg^{-1} and 4000 W kg^{-1}, respectively. More importantly, the full cell was capable to light a neon sign consisting of 57 LEDs and power the LED green light of a wearable watch (**Fig. 5a**). Yu and co-workers reported a flexible nitrogen and oxygen dual-doped carbon-coated graphene foam film (**Fig. 5b)**.[69] In preparation, graphene foam was synthesized by the pyrolysis of CH_4 using commercial nickel foam as a template, and then, graphene@Ni foam was coated by PPy by electrochemical polymerization. Finally, NOC@GF was obtained after etching and heat treatment. Serving as a PIB anode, it displayed a high reversible capacity (319 mA h g^{-1} at 0.1 mA g^{-1} with capacity retention of 94.9% after 550 cycles) and excellent rate capability (123 mA h g^{-1} at 5.0 mA g^{-1}). Impressively, its capacity still reached 281 mA h g^{-1} at a current density of 1 A g^{-1} after 5500 cycles with Coulombic efficiency (CE) nearly approaching 100% and capacity retention of 98.1% (**Fig. 5c**). The excellent electrochemical properties were attributed to the high electric conductivity of graphitic carbon, abundant active sites of amorphous heteroatoms doping carbon layers, and the favorable K-intercalation of 3D interconnected structure of NOC@GF. As for carbon sponges, several works took it as a substrate to load active materials to fabricate flexible PIB electrodes. In general, carbon sponges are obtained by the pyrolysis of a polymer sponge in an inert atmosphere, during which heteroatom N from polymers themselves can be doped into carbon sponges. To anchor active materials, hydro(solvo)thermal, electrodeposition, *etc*. should be

further performed. For example, high-temperature calcination combing a solvothermal method adopted by Yu *et al*. to synthesize ultrathin $CoSe_2$ nanosheets coated 3D N-doped carbon foam (CSNS/NCF) (**Fig. 5d**).[45] The as-prepared sample had good flexibility, and could fully recover to its original shape after being bent to different angles, as illustrated in **Fig. 5e**. The sample with the optimized solvothermal temperature had great long-term cycling life (212 mA h g^{-1} at 1000 mA g^{-1} after 1000 cycles) and great rate performance (225 mA h g^{-1} at 2000 mA g^{-1}).

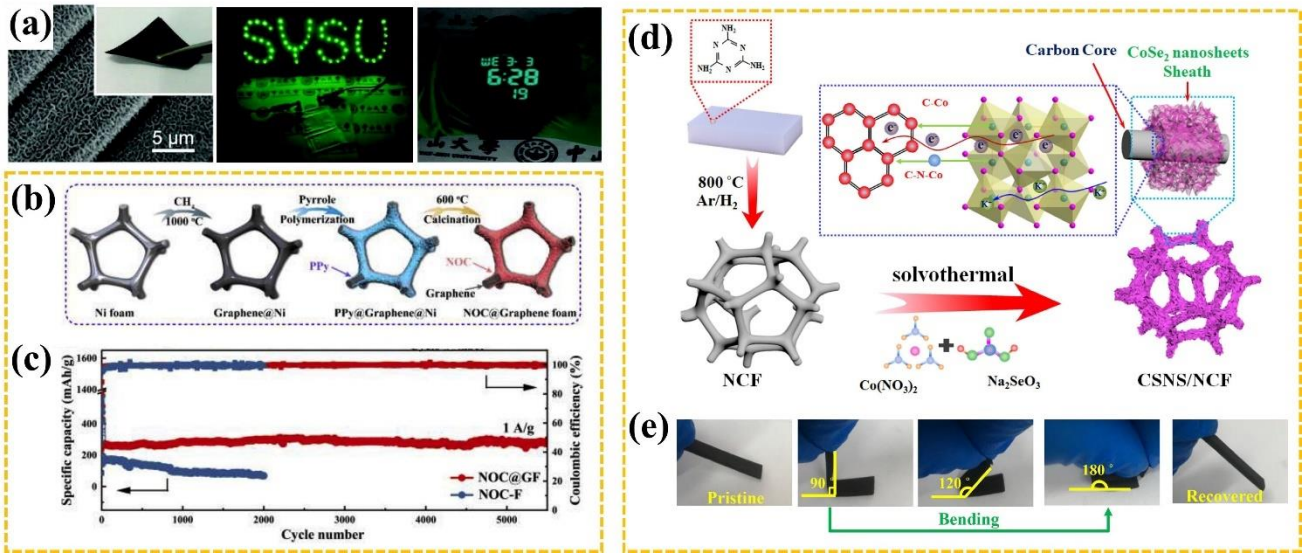

Fig. 5 (a) SEM image of N, P-VG@CC and picture of a neon sign and a watch powered by the KPB//N, P-VG@CC full cell.[13] (Reprinted with permission, Copyright 2019, Wiley). (b) The schematic illustration of fabrication process of NOC@GF sample. (c) Long-term cycling stability and CE at 1 A g^{-1} of NOC@GF.[69] (Reprinted with permission, Copyright 2020, Elsevier). (d) Schematic image for synthesizing CSNS/NCF products. (e) Photographs of flexibility test using CSNS/NCF-160.[45] (Reprinted with permission, Copyright 2020, Elsevier).

3.1.6. Hybrid carbon-based flexible electrodes

Sometimes, the above carbon materials are used in combination rather than individually with a view to achieving synergetic improvement. For example, graphene has great electrochemical ion storage ability theoretically, but, in fact, the electrochemical performance of graphene films is unsatisfactory due to the barrier of electron and ion diffusion in the cross-plane direction. In this case, Han and co-workers fabricated a rGO/CNT hybrid paper by introducing CNTs **(Fig. 6a)**.[23] Highly conductive CNTs could not only prevent restacking and increase the interlayer spacing of graphene, thus providing more active sites for ions, but also bridge graphene layers to facilitate electron and ion transport in the cross-plane

direction. All rGO/CNT hybrid papers with different weight ratios (10%, 20%, and 30%) exhibited better K storage capability than pure rGO papers **(Fig. 6b−c)**.

Electrospinning with subsequent carbonization is an easy method to produce CNF films; however, their graphitization degree is usually low, which reduces the electrical conductivity and mechanical properties of CNF films.[70-71] To offset this issue, Chen *et al*. introduced CNTs with outstanding mechanical properties and conductivity into electrospun CNFs, as shown in **Fig. 6d**.[72] Meanwhile, ZnO was utilized as a sacrificial agent to construct multi-channel hollows for enlarging active sites, and sulfur powders were employed as a sulfur-doping precursor to increase the layer spacing, conductivity, and chemical reactivity. When served as a PIB anode, the free-standing S/N doped CNT/CNF electrode showed a high discharge capacity (212.5 mA h g^{-1} at 1 A g^{-1} after 1000 cycles), long cycling life (100.1 mA h g^{-1} at 5 A g^{-1} after 5000 cycles), and high rate performance (108.7 mA h g^{-1} at 5 A g^{-1}). Zheng and co-workers reported graphene/porous nitrogen-doped carbon nanofibers (G-PCNFs) and investigated their electrochemical performance **(Fig. 6e)**.[73] Reversible capacities of 358 and 276 mA h g^{-1} were achieved after 200 and 2000 cycles at 0.1 and 2 A g^{-1}, respectively, which were higher than those of all the control samples (PCNFs, G-CNFs, and CNFs). Its rate capability was the best among all the prepared samples. The authors pointed out that the enhanced performance was attributed to the improvement of the electronic conductivity provided by graphene and a large number of mesopores exposing abundant N-doped active sites for the adsorption of K^+.

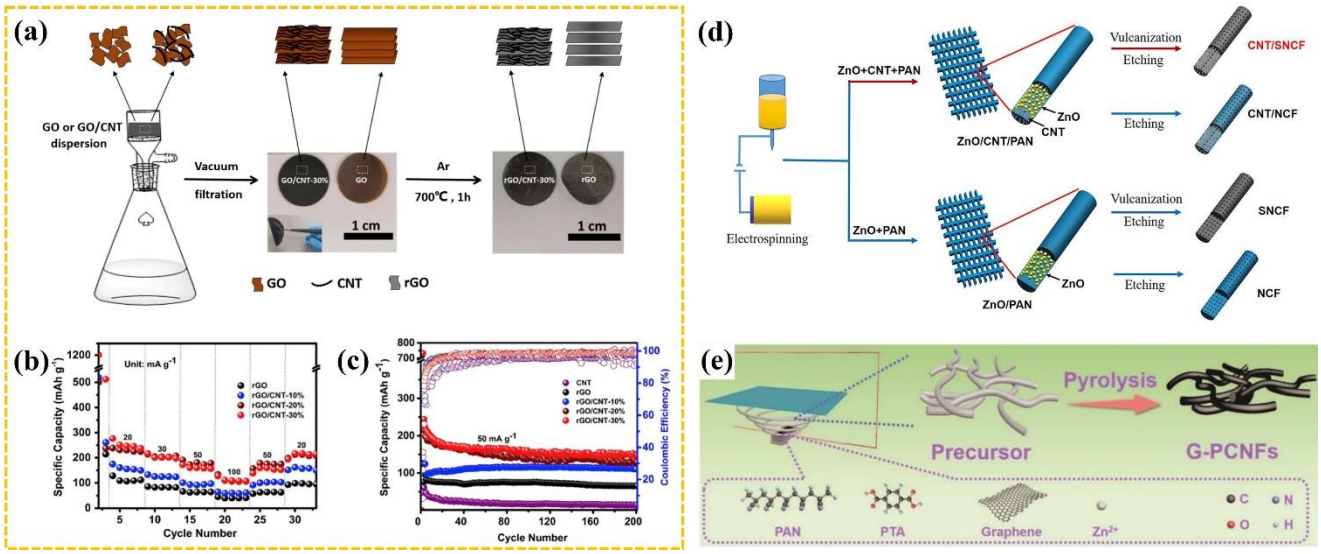

Fig. 6 (a) Fabrication process for rGO and rGO/ CNT hybrid papers and typical digital photographs of the papers. (b) Rate capability and (c) cycling performance of rGO and rGO/CNT hybrid papers.[23]

(Reprinted with permission, Copyright 2020, Elsevier). (d) Schematic illustration for the synthesis of CNT/SNCF, CNT/NCF, SNCF and NCF composites.[72] (Reprinted with permission, Copyright 2021, American Chemical Society). (e) Schematic illustration of the fabrication of G-PCNFs.[73] (Reprinted with permission, Copyright 2021, The Royal Society of Chemistry).

Table 2 Recent progress on electrochemical properties of carbon-based electrodes for flexible PIBs.

Materials	Electrolytes	Voltage range	Cycling	Rate
Anodes				
N, O-rich CNFs[74]	0.8 M KPF_6 EC/DEC (1:1)	0.005−3.0 V	170 mA h g^{-1}@1C/1900 cycles	110 mA h g^{-1}@10C
Porous CNFs[49]	0.8 M KPF_6 EC/DEC (1:1)	0−3.0 V	270 mA h g^{-1}@0.02 A g^{-1}/80 cycles 211 mA h g^{-1}@0.2 A g^{-1}/1200 cycles	100 mA h g^{-1}@7.7 A g^{-1}
Hierarchically porous N-doped CNFs[75]	1.0 M KPF_6 EC/DMC (1:1)	0.01−3.0 V	194 mA h g^{-1}@0.1 A g^{-1}/110 cycles 154 mA h g^{-1}@0.2 A g^{-1}/90 cycles 135 mA h g^{-1}@0.5 A g^{-1}/200 cycle	
Multichannel CNFs[50]	0.8 M KPF_6 EC/DEC (1:1)	0.01−3.0 V	110.9 mA h g^{-1}@2.0 A g^{-1}/2000 cycles	143.2 mA h g^{-1}@2.0 A g^{-1}
Necklace-like N-doped hollow carbon with hierarchical pores[51]	0.8 M KPF_6 EC/DEC (1:1)	0.01−2.5 V	225.4 mA h g^{-1}@0.2 A g^{-1}/1000 cycles 161.3 mA h g^{-1}@1.0 A g^{-1}/1600 cycles	204.8 mA h g^{-1}@2.0 A g^{-1}
Hierarchical porous CNFs[76]	0.8 M KPF_6 EC/DEC (1:1)	0.01−2.5 V	238.6 mA h g^{-1}@1.0 A g^{-1}/200 cycles 196.7 mA h g^{-1}@2.0 A g^{-1}/2000 cycles	204.6 mA h g^{-1}@2.0 A g^{-1}
Ultrafine Sb nanocrystals/nanochannel-containing CNFs[56]	3.0 M KFSI DME	0.01−3.0 V	393 mA h g^{-1}@0.2 A g^{-1}/100 cycles 225 mA h g^{-1}@1.0 A g^{-1}/2000 cycles	145 mA h g^{-1}@5.0 A g^{-1}
Sb nanoparticles/carbon porous nanofibers[77]	1.0 M KFSI EC/DEC (1:1)	0.01−3.0 V	421.4 mA h g^{-1}@0.1 A g^{-1}/100 cycles 264.0 mA h g^{-1}@2.0 A g^{-1}/500 cycles	112.5 mA h g^{-1}@5.0 A g^{-1}
ReS_2/N-doped CNFs[78]	0.8 M KTFSI DME	0.01−3.0 V	253 mA h g^{-1}@0.2 A g^{-1}/100 cycles	
Dual anionic vacancie-rich MoSSe/CNFs[37]	0.8 M KPF_6 EC/DEC (1:1)	0.01−3.0 V	220.5@0.5 A g^{-1}/1000 cycles	202.6 mA h g^{-1}@5.0 A g^{-1}
$Co_{0.85}Se$@C/CNFs[39]	2.0 M KFSI DME	0.01−2.6 V	353 mA h g^{-1}@0.2 A g^{-1}/100 cycles 299 mA h g^{-1}@1.0 A g^{-1}/400 cycles	166 mA h g^{-1}@5.0 A g^{-1}
N-rich Cu_2Se/C nanowires[79]	1.0 M KFSI PC/EC (1:1)	0.1−2.5 V	190 mA h g^{-1}@0.1 A g^{-1}/200 cycles 78 mA h g^{-1}@2.0 A g^{-1}/1200 cycles	104 mA h g^{-1}@2.0 A g^{-1}

SnS_2@CNFs[26]	0.8 M KPF_6 EC/DEC (1:1)	0.01−3.0 V	342.8 mA h g^{-1}@0.1 A g^{-1}/200 cycles 183.1 mA h g^{-1}@2.0 A g^{-1}/1000 cycles	264.3 mA h g^{-1}@2.0 A g^{-1}
V_2O_3@ porous N-doped CNFs[57]	0.8 M KPF_6 EC/DEC (1:1)	0.01−3.0 V	230 mA h g^{-1}@0.05 A g^{-1}/500 cycles	134 mA h g^{-1}@1.0 A g^{-1}
MoP ultrafine nanoparticles/ N, P codoped CNFs[59]	0.8 M KPF_6 EC/DEC (1:1)	0.01−3.0 V	230 mA h g^{-1}@0.1 A g^{-1}/200 cycles	223 mA h g^{-1}@2.0 A g^{-1}
Fe_2P nanoparticles-doped carbon nanofibers[80]	0.8 M KPF_6 EC/DEC (1:1)	0.01−2.5 V	379.2 mA h g^{-1}@0.2 A g^{-1}/100 cycles 179.6 mA h g^{-1}@2.0 A g^{-1}/2000 cycles	211.8 mA h g^{-1}@2.0 A g^{-1}
Coal liquefaction residue/CNFs[81]	0.5 M KPF_6 EC/DEC (1:1)	0.01−3.0 V	98% capacity retention@0.05 A g^{-1}/320 cycles	103 mA h g^{-1}@1.0 A g^{-1}
$Mn_{0.5}Ti_2(PO_4)_3$/CNFs[58]	1.0 M KFSI EC/DEC (1:1)	0.01−3.0 V	196.6 mA h g^{-1}@0.02 A g^{-1}/100 cycles 53.2 mA h g^{-1}@1.0 A g^{-1}/2000 cycles	87.5 mA h g^{-1}@1.0 A g^{-1}
V_2O_3/CNFs[82]	3.0 M KFSI EC/DEC (1:1)	0.01−3.0 V	380 mA h g^{-1}@0.1 A g^{-1}/500 cycles 98% capacity retention@1.0 A g^{-1}/2500 cycles	175 mA h g^{-1}@10.0 A g^{-1}
$CoSe_2$/N-doped CNT framework[43]	0.8 M KPF_6 in EC/DEC (1:1)	0.01−2.5 V	253 mA h g^{-1}@0.2 A g^{-1}/100 cycles 173 mA h g^{-1}@2.0 A g^{-1}/600 cycles	196 mA h g^{-1}@2.0 A g^{-1}
Potassium titanate/rGO[35]	0.8 M KPF_6 EC/DEC (1:1)	0.05−2.5 V	75 mA h g^{-1}@2.0 A g^{-1}/700 cycles	84 mA h g^{-1}@1.0 A g^{-1}
Sulfur-mediated 3D graphene aerogel[83]	0.8 M KPF_6 EC/DEC (1:1)	0.01−3.0 V	320 mA h g^{-1}@0.1 A g^{-1}/500 cycles 173 mA h g^{-1}@1.0 A g^{-1}/800 cycles	178 mA h g^{-1}@5.0 A g^{-1}
Carbon dots@rGO[84]	0.8 M KPF_6 in EC/DMC (1:1) with 5 vol% FEC	0.01−3.0 V	244 mA h g^{-1}@0.2 A g^{-1}/840 cycles	221 mA h g^{-1}@0.5 A g^{-1}
3D graphene skeleton/FeP[67]	1.0 M KPF_6 in EC/DMC (1:1)	0.01−3.0 V	327 mA h g^{-1}@0.1 A g^{-1}/300 cycles 127 mA h g^{-1}@2.0 A g^{-1}/2000 cycles	101 mA h g^{-1}@5.0 A g^{-1}
Bi nanosheet/rGO[68]	1.0 M KPF_6 DME	0.1−1.5 V	272 mA h g^{-1}@0.5 A g^{-1}/90 cycles	100 mA h g^{-1}@10.0 A g^{-1}

Sb_2Se_3@holey rGO[85]	0.8 M KFSI EC/DEC (1:1)	0.1−2.2 V	382.8 mA h g^{-1}@0.1 A g^{-1}/500 cycles	73 mA h g^{-1}@2.0 A g^{-1}
Sub-micro carbon fiber@CNTs[86]	0.8 M KPF_6 EC/DEC (1:1)	0.01−2.0 V	193 mA h g^{-1}@1C/300 cycles	108 mA h g^{-1}@5C
rGO/CNT[23]	0.8 M KPF_6 EC/DMC (1:1)	0.05−2.5 V	223 mA h g^{-1}@0.05 A g^{-1}/200 cycles	110 mA h g^{-1}@0.1 A g^{-1}
Sb-graphene-CNFs[87]	0.8 M KPF_6 EC/DEC (1:1)	0.01−3.0 V	204.95 mA h g^{-1}@0.1 A g^{-1}/100 cycles	120. 83 mA h g^{-1}@1.0 A g^{-1}
N-doped CoSb@C nanofibers[88]	0.8 M KFSI EC/DEC (1:1)	0.1−3.0 V	449 mA h g^{-1}@0.1 A g^{-1}/160 cycles 250 mA h g^{-1}@1.0 A g^{-1}/500 cycles	160 mA h g^{-1}@2.0 A g^{-1}
Multi-channel hollow CNT/CNF[72]	0.8 M KPF_6 EC/DEC (1:1)	0.01−3.0 V	315.9 mA h g^{-1}@0.1 A g^{-1}/300 cycles 100.1 mA h g^{-1}@5.0 A g^{-1}/5000 cycles	108.7 mA h g^{-1}@5.0 A g^{-1}
Graphene/ porous nitrogen-doped CNFs[73]	3.0 M KFSI EC/DEC (1:1)	0.01−3.0 V	358 mA h g^{-1}@0.1 A g^{-1}/200 cycles 276 mA h g^{-1}@2.0 A g^{-1}/2000 cycles	101 mA h g^{-1}@5.0 A g^{-1}
$Na_2Ti_3O_7$/N-doped carbon sponge[89]	1.0 M KPF_6 EC/DEC (1:1)	0.01−2.6 V	88.9 mA h g^{-1}@0.1 A g^{-1}/1555 cycles	25 mA h g^{-1}@1.0 A g^{-1}
CNT-modified graphitic carbon foam[90]	0.7 M KPF_6 EC/DEC (1:1)	0.01−2.5 V	226 mA h g^{-1}@0.1 A g^{-1}/800 cycles 127 mA h g^{-1}@0.5 A g^{-1}/2000 cycles	56 mA h g^{-1}@2.0 A g^{-1}
N, P-doped graphene/carbon cloth[13]	1.0 M KPF_6 EC/DMC (1:1) with 5 vol% FEC	0.01−3.0 V	281.1 mA h g^{-1}@0.25 A g^{-1}/1000 cycles 180 mA h g^{-1}@0.5 A g^{-1}/1000 cycles 142.4 mA h g^{-1}@1.0 A g^{-1}/1000 cycles	156.1 mA h g^{-1}@2.0 A g^{-1}
$CoSe_2$/N-doped carbon foam[45]	0.8 M KPF_6 EC/DEC (1:1)	0.01−2.6 V	335 mA h g^{-1}@0.05 A g^{-1}/200 cycles 198 mA h g^{-1}@1.0 A g^{-1}/1000 cycles	226 mA h g^{-1}@2.0 A g^{-1}
SnO_2@Carbon foam[38]	0.8 M KPF_6 EC/DEC (1:1)	0.01−3.0 V	398.8 mA h g^{-1}@0.1 A g^{-1}/150 cycles 231.7 mA h g^{-1}@1.0 A g^{-1}/400 cycles	143.5 mA h g^{-1}@5.0 A g^{-1}
MoS_2/N-doped carbon sponge[40]	0.8 M KPF_6 EC/DEC (1:1)	0.01−2.6 V	374 mA h g^{-1}@0.05 A g^{-1}/200 cycles 212 mA h g^{-1}@1.0 A g^{-1}/1000 cycles	225 mA h g^{-1}@2.0 A g^{-1}

N, O dual-doped carbon@graphene foam[69]	0.7 M KPF_6 EC/DEC (1:1)	0.01−3.0 V	319 mA h g^{-1}@0.1 A g^{-1}/550 cycles 281 mA h g^{-1}@1.0 A g^{-1}/5500 cycles	123 mA h g^{-1}@5.0 A g^{-1}
Graphite nanoflake/MXene[91]	1.0 M KFSI PC/EC (1:1)	0.01−2.5 V	253.8 mA h g^{-1}@0.05 A g^{-1}/100 cycles	45.2 mA h g^{-1}@0.5 A g^{-1}
N-rich carbon membranes[92]	0.8 M KPF_6 EC/DEC (1:1)	0.01−3.0 V	146 mA h g^{-1}@2.0 A g^{-1}/500 cycles	104 mA h g^{-1}@2.0 A g^{-1}
N-doping hollow neuronal carbon skeleton[93]	0.8 M KPF_6 EC/DEC (1:1)	0.01−3.0 V	198 mA h g^{-1}@0.1 A g^{-1}/200 cycles 134 mA h g^{-1}@0.5 A g^{-1}/500 cycles	110 mA h g^{-1}@1.0 A g^{-1}
FeP coated in N/P co-doped carbon shell nanorods[94]	2.0 M KFSI PC/EC (1:1)	0.01−3.0 V	1330.5 mA h g^{-1}@0.1 A g^{-1}/35 cycles 625.3 mA h g^{-1}@0.3 A g^{-1}/100 cycles 388.8 mA h g^{-1}@0.5 A g^{-1}/400 cycles	346.9 mA h g^{-1}@1.5 A g^{-1}
S-/O-doped graphitic carbon network[95]	0.8 M KPF_6 EC/DEC (1:1)	0.01−3.0 V	298.3 mA h g^{-1}@0.05 A g^{-1}/300 cycles 125.9 mA h g^{-1}@1.0 A g^{-1}/5000 cycles 91.1 mA h g^{-1}@5.0 A g^{-1}/10000 cycles	149.7 mA h g^{-1}@5 A g^{-1}
Cathodes				
$K_{0.5}V_2O_5$/CNTs[61]	0.8 M KPF_6 EC/DEC (1:1)	1.53.8 V	90 mA h g^{-1}@0.05 A g^{-1}/100 cycles 51 mA h g^{-1}@0.5 A g^{-1}/300 cycles	62 mA h g^{-1}@0.5 A g^{-1}

3.2. PIHCs

3.2.1. Potassium storage mechanisms

PIHCs have the same assembling components as PIBs. According to whether the electrolyte is consumed during electrochemical processes, the electrochemical K storage mechanism of PIHCs can be classified into electrolyte-consuming, ion exchange, and hybrid mechanisms. (1) Electrolyte-consuming mechanisms. Battery-type materials are used as anodes, while capacitor-type materials act as cathodes. In charging processes, K^+ is inserted into anodes, while anions (PF_6^-, FSI^-, *etc*) are absorbed on the surface of cathodes. In discharging processes, K^+ and anions go back to electrolytes to reach a charge balance state. (2) Ion exchange mechanisms. K-containing battery materials and capacitor-type materials are the cathode and the anode of PIHCs. In this system, electrolytes are only used to transport K^+ and its concentration keeps constant during electrochemical reactions. K^+ is extracted from the cathode during charging, and meanwhile, the released K^+ is absorbed on the anode. The behavior of K^+ is the opposite during charging. (3) Hybrid mechanisms. The key feature of this kind of PIHCs is that one or two of electrodes use the material with both battery- and capacitor-behaviors.[96]

3.2.2. Carbon-based flexible electrodes

CNF-based flexible films have been also widely utilized as PIHC electrodes. Wen *et al*. took a dimethylformamide solution containing ZIF-8, triphenylphosphine, urea, and PAN as an electrospinning precursor constructing phosphorus/nitrogen co-doped hierarchical porous CNFs (PN-HPCNFs), as illustrated in **Fig. 7a**.[97] PN-HPCNFs exhibited a 3D interconnected network structure with successive macropore cavities that was favorable for the accessibility of ion and electron transfer. In comparison to HPCNFs without N or P/N doping, PN-HPCNFs had wider interlayer spacing, which is beneficial to the reversible insertion/extraction of large-sized K^+. P and N co-doping resulting in abundant defects and extra active sites could reduce K^+ diffusion barrier and improve capacitance contribution. Consequently, PN-HPCNFs exhibited excellent K storage capability when evaluated in PIBs as an anode. Furthermore, a PIHC full cell was assembled, where activated PN-NPCNFs (APN-NPCNFs) acted as the cathode. A maximum energy density of 191 W h kg^{-1} was achieved at a power density of 100 W kg^{-1}. When the power density increased to 7560 W kg^{-1}, the energy density still retained 86 W h kg^{-1}. More impressively, capacity retention reached 82.3% after 8000 cycles, corresponding to only

0.0022% fading per cycle. The full cell could light a pattern consisting of 43 LEDs and derived a miniature windmill (**Fig. 7b**). Recently, MC-CNF composite films have been investigated as PIHC electrodes. Zhang and co-workers designed tiny carbon nanotubes capped with nickel sulfide nanocrystallites (NSCN hollow fiber).[98] The authors investigated the physicochemical properties of three nickel sulfide nanocrystallites with different phases (α-NiS, β-NiS, and NiS_2) inside the NSCN fiber. Both theoretical and experimental results indicated that α-NiS had the best kinetics and durability. Considering the superior comprehensive properties and good mechanical characteristics, a full cell that the α-NiS-based NSCN hollow fibers and central hollow carbon fibers were used as the anode and the cathode was assembled. The full cell showed an energy density of 187 W h kg^{-1} at a power density of 1.7 kW kg^{-1}, and the energy density was as high as 127 W h kg^{-1} even at 8.4 kW kg^{-1}. Moreover, a sandwich-type flexible PIHC was assembled using the same materials as the electrodes and a perfluorinated sulfonic resin polymer as the electrolyte. The mechanical and electrochemical properties of the flexible PIHC are shown in **Fig. 7c−d**. More importantly, it exhibited good electrochemical performance even at low temperatures (**Fig. 7e−f**).

Biomass carbon materials have been explored as electrode materials for flexible PIHCs because of their wide availability and low cost. For example, Ye's group constructed a flexible freestanding electrode consisting of porous carbon tubes using Metaplexis japonica fluffs (FSF-PCTs) as a precursor by successive microwave treatment, carbonization, and CO_2 perforation. FSF-PCT as both the anode and the cathode presented superior electrochemical performance in specific capacities, cycling life, and rate performance. In this case, a symmetrical PIHC using FSF-PCTs as both the anode and the cathode is assembled. The all-carbon-based symmetrical PIHC delivered an energy density of 117.8 W h kg^{-1} at a power density of 450 W kg^{-1} and possessed favorable cycling stability (37 mA h g^{-1} at 1 A g^{-1} after 1500 cycles). Paper is also promising material for the preparation of flexible carbon electrodes due to their industrial availability, low cost, environmental friendliness, and recyclability. Wang's group designed a flexible hard carbon microbelt (HCMB) film using sanitary tissue paper as a precursor through simple carbonization.[15] The HCMB film had mechanical flexibility and could be bent into any shape without breaking (**Fig. 7g**). The HCMB film inherited the primary morphology of tissue paper and exhibited high electronic conductivity and a low surface area. The HCMB anode delivered a larger charge specific capacity of 204 mAh g^{-1} at 100 mA g^{-1} below 1.00 V compared with graphite (191 mAh

g^{-1}) and soft carbon (156 mAh g^{-1}). The initial CE was as high as 88% (graphite: 46%, soft carbon: 35%). Moreover, both rate and cycling performance were satisfactory. Over 75% of the discharge plateau located below 0.25 V endowed the HCMB//Activated carbon full cell with a high operating working voltage (4.5 V) and a large energy density of 152 W h kg^{-1})

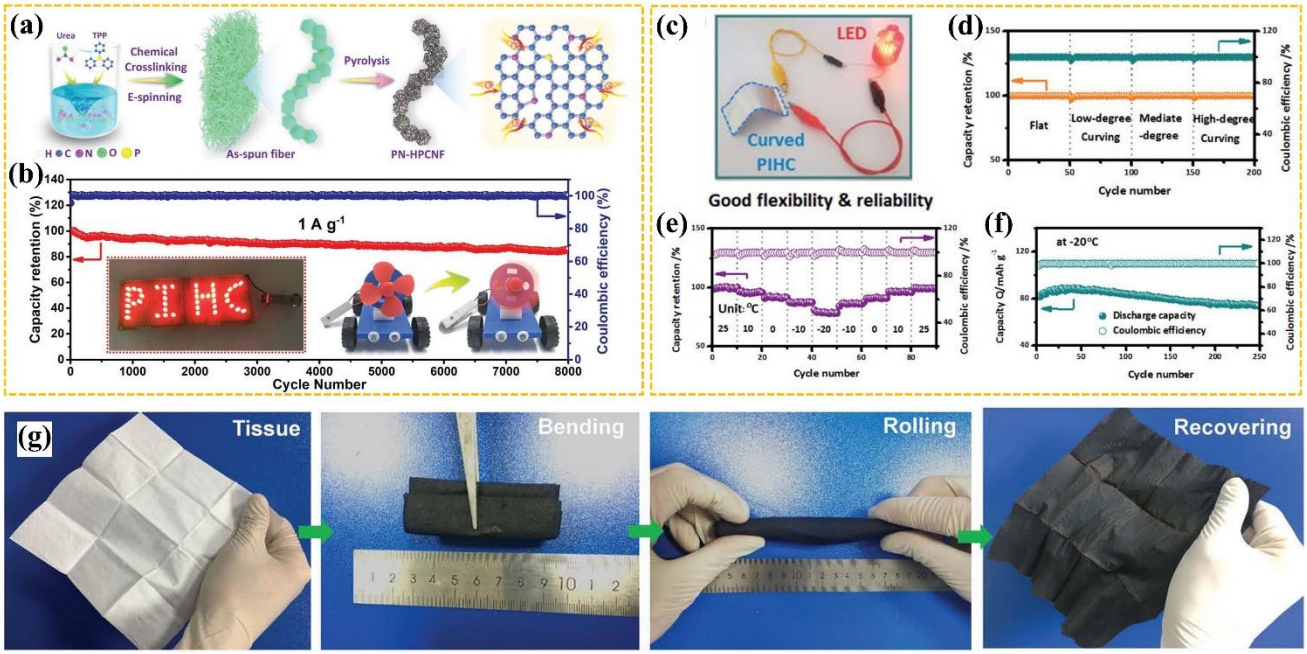

Fig. 7 (a) Schematic diagram for the preparation of PN-HPCNF. (b) Long-term cycle performance tests of the PIHC. Inset: Photograph of LED arrays and miniature windmill powered by APN-HPCNF//PN-HPCNF PIHCs.[97] (Reprinted with permission, Copyright 2020, The Royal Society of Chemistry). (c) Digital photo of the LED light powered by a curved α-NiS-NSCN//CHCF full PIHC. (d) Cycling performance of the flexible PIHC cell in flat and diverse bending states. (e) Cycling performance of the flexible PIHC cell at different temperatures from 25 to −20 °C. (f) Long-term cycling properties (at 1 A g^{-1}) of the flexible PIHC device at −20 °C.[98] (Reprinted with permission, Copyright 2022, The Royal Society of Chemistry). (g) Demonstrations of tissue and the HCMB paper at different bending states.[15] (Reprinted with permission, Copyright 2022, The Royal Society of Chemistry).

Table 3 Recent progress on electrochemical performance of carbon-based electrodes for flexible PIHCs.

Materials	Electrolytes	Electrochemical performance						
		Half cell			Full cell			
		Voltage range	Cycling	Rate	Coupling electrode/Device type	Voltage range	Cycling	Rate
Anodes								
$NbSe_2$/N, Se co-doped CNFs[99]	5.0 M KFSI EC/DMC (1:1)	0.01–3.0 V	288 mA h g^{-1}@0.05 A g^{-1} 51 mA h g^{-1}@0.2 A g^{-1}	78 mA h g^{-1}@2.0 A g^{-1}	Activated carbon/Coin cell		20 W h kg^{-1}@2.0 A g^{-1}/10000 cycles	4000 W h kg^{-1}@4.0 A g^{-1}
Hierarchical porous CNFs[97]	1.0 M KFSI DGM	0.01–3.0 V	305 mA h g^{-1}@0.2 A g^{-1}/300 cycles	194 mA h g^{-1}@10.0 A g^{-1}	Activated hierarchical porous CNFs/Coin cell		82.3% capacity retention@1.0 A g^{-1}/8000 cycles	191 W h kg^{-1}@100 W kg^{-1}
Hollow MoS_2 Spheres/CNFs[100]	1.0 M KFSI EC/DMC (1:1)	0.01–3.0 V	366.1 mA h g^{-1}@0.1 A g^{-1}/100 cycles 187.7 mA h g^{-1}@2.0 A g^{-1}/5000 cycles	184.7 mA h g^{-1}@10.0 A g^{-1}	Activated carbon fiber membrane/Coin cell	0.01–4.0 V	81.8% capacity retention@4.0 A g^{-1}/10000 cycles	51 W h kg^{-1}@8348 W kg^{-1}
B, F co-doped CNFs[101]	1.0 M KFSI EC/DEC (1:1)	0–3.0 V	259 mA h g^{-1}@0.1 A g^{-1}/120 cycles 176 mA h g^{-1}@1.0 A g^{-1}/6000 cycles	150 mA h g^{-1}@5.0 A g^{-1}	Activated carbon/Coin cell	0.01–4.0 V	78% capacity retention@1.0 A g^{-1}/4000 cycles	23 W h kg^{-1}@14710 W kg^{-1}
α-NiS nanocrystallite/CNTs[98]	1.0 M KPF_6 EC/DEC (1:1)				Central hollow carbon fiber/Coin cell		85.6% capacity retention@2.0 A g^{-1}/3500 cycles	127 W h kg^{-1}@8400 W kg^{-1}
S, N-co-doped kinked CNFs[102]	3.0 M KFSI DME	0.01–3.0 V	330 mA h g^{-1}@1.0 A g^{-1}/2000 cycles	270 mA h g^{-1}@2.0 A g^{-1}	Activated carbon/Pouch cell	0.1–4.0 V	88% capacity	77 mA h g^{-1}@5.0 A g^{-1}

							retention@10.0 A g^{-1}/4000 cycles	
Porous carbon tubes[103]	1.0 M KPF_6 EC/DEC (1:1)	0.01–3.0 V	300 mA h g^{-1}@0.05 A g^{-1}/100 cycles 239.6 mA h g^{-1}@0.2 A g^{-1}/500 cycles 170.6 mA h g^{-1}@1.0 A g^{-1}/1200 cycles	137.8 mA h g^{-1}@2.0 A g^{-1}	Porous carbon tubes/Coin cell	0.01–4.0 V	37 mA h g^{-1} (51 W h kg^{-1})@1.0 A g^{-1}/1500 cycles	36.8 mA h g^{-1}@3.0 A g^{-1}
1D $K_2Ti_6O_{13}$/3D porous carbon framework[104]	0.8 M KPF_6 EC/DEC (1:1)		60% capacity retention@1.0 A g^{-1}/1000 cycles	45 mA h g^{-1}@2.0 A g^{-1}	Activated carbon/Coin cell	0.1–3.5 V	60% capacity retention@1.0 A g^{-1}/1000 cycles	
					Activated carbon-MXene-CNF/Fiber-shaped cell	0.1–3.5 V	64.3% capacity retention@0.1 A cm^{-3}/2000 cycles	12.1 μW h cm^{-3}@2.0 A g^{-1} 1.9 mW h cm^{-3}@2.0 A g^{-1}
Tissue-derived carbon microbelt paper[15]	0.8 M KPF_6 EC/DEC (1:1)	0.01–3.0 V	246 mA h g^{-1}@0.1 A g^{-1}/400 cycles 174 mA h g^{-1}@1.0 A g^{-1}/750 cycles	112 mA h g^{-1}@2.0 A g^{-1}	Activated carbon/Pouch cell	2.5–4.5 V	90% capacitance retention@20 mV s^{-1}/1000 cycles	112 W h kg^{-1}@17500 W kg^{-1}
Aligned hybrid fibers filled with $FeSe_2$@C[105]					Hierarchical fibers/Coin cell			66 W h kg^{-1}@20000 W kg^{-1}
Bead-like coal-derived carbon[106]	1.0 M KPF_6 in EC/DMC/EMC (1:1:1)	0.01–3.0 V	204.9 mA h g^{-1}@0.2 A g^{-1}/100 cycles 131.4 mA h g^{-1}@1.0 A g^{-1}/2000 cycles	104.5 mA h g^{-1}@5.0 A g^{-1}	Activated carbon/Coin cell	0.5–4.0 V	52 W h kg^{-1}@5 A g^{-1}/1000 cycles	52 W h kg^{-1}@2187 W kg^{-1}

3.3. K-S/Se batteries

3.3.1. Potassium storage mechanisms

The cell configuration of K-S/Se batteries is composed of a S/Se cathode, a metallic K anode, a separator, and an organic electrolyte. The charging/discharging process involves reversible plating/stripping of metallic K on the negative side and oxidation/reduction reactions of S/Se on the positive side. In K-S batteries, solid S_8 is reduced to soluble high-order potassium polysulfides K_2S_n ($5<n<6$) and insoluble low-order potassium polysulfides K_2S_n ($1<n<4$) during discharging. During charging, the discharged products are partially oxidized to K_2S_5 and K_2S_6.[8, 107] As for K-Se batteries, the final discharged product K_2Se has been demonstrated by many works, but whether there are intermediate processes producing potassium polyselenides is still being debated.[108] In the following charging process, the produced K_2Se at the fully discharged state is converted to Se.[108-110] Until now, the specific reaction processes have been unclear in both K-S and K-Se batteries, and more exploratory studies are needed.

3.3.2. Carbon-based flexible electrodes

To date, there are limited reported works on carbon-based flexible electrodes for K-S/Se batteries, most of which are based on CNF films prepared by electrospinning. Yu's group developed N/O dual-doped CNFs with interconnected micro/mesopores (MMCFs) by carbonizing electrospun ZIF-8/PVP nanofibers and used them as a host material to manipulate the Se molecular configuration of flexible K-Se batteries (**Fig. 8a**).[111] The micropores could confine small $Se_{2–3}$ molecules, inhibiting the formation of polyselenides and serving as a physical barrier to maintaining cycling stability. As for the mesopores, they could confine long chain $Se_{4–7}$, confirming a high Se loading and contributing to a high discharge voltage of Se@MMCFs. The N/O co-doping and the 3D interconnected structure were able to improve the electrical conductivity and keep the structural integrity during reaction processes. Based on these merits, the optimal electrode ($Se_{2–3}$/$Se_{4–7}$-MMCFs) achieved satisfactory stability (395 mA h g^{-1} at 1 A g^{-1} after 2000 cycles) and a high specific energy density of 400 W h kg^{-1}.

Except for CNFs, flexible electrodes based on other carbon materials have been developed. Yu and co-workers encapsulated Se into CNTs interwoven N, O dual-doped porous carbon nanosheets (Se@NOPC-CNT) to construct a flexible free-standing Se/carbon composite film (**Fig. 8b**).[109] N, O dual-doped porous carbon nanosheets were derived from chestnut inner shells, and NOPC-CNT was obtained by vacuum filtration. It is believed that the electrode is low cost and readily scalable. Zhu *et*

al. adopted three types of activated carbon fiber (ACF) cloth with different specific surface areas and microstructures as porous carbon matrix of K-S battery cathodes (**Fig. 8c**).[48] By comparing their electrochemical performance, the authors found that the controllable physical confinement and chemical adsorption toward soluble polysulfides could be achieved by adjusting the specific surface area, porous architectures, and surface functional sites of the ACF@S composite cathode. In addition, reducing the cloth thickness and the fiber diameter was conducive to increasing the operation stability and the sulfur utilization of composite cathodes.

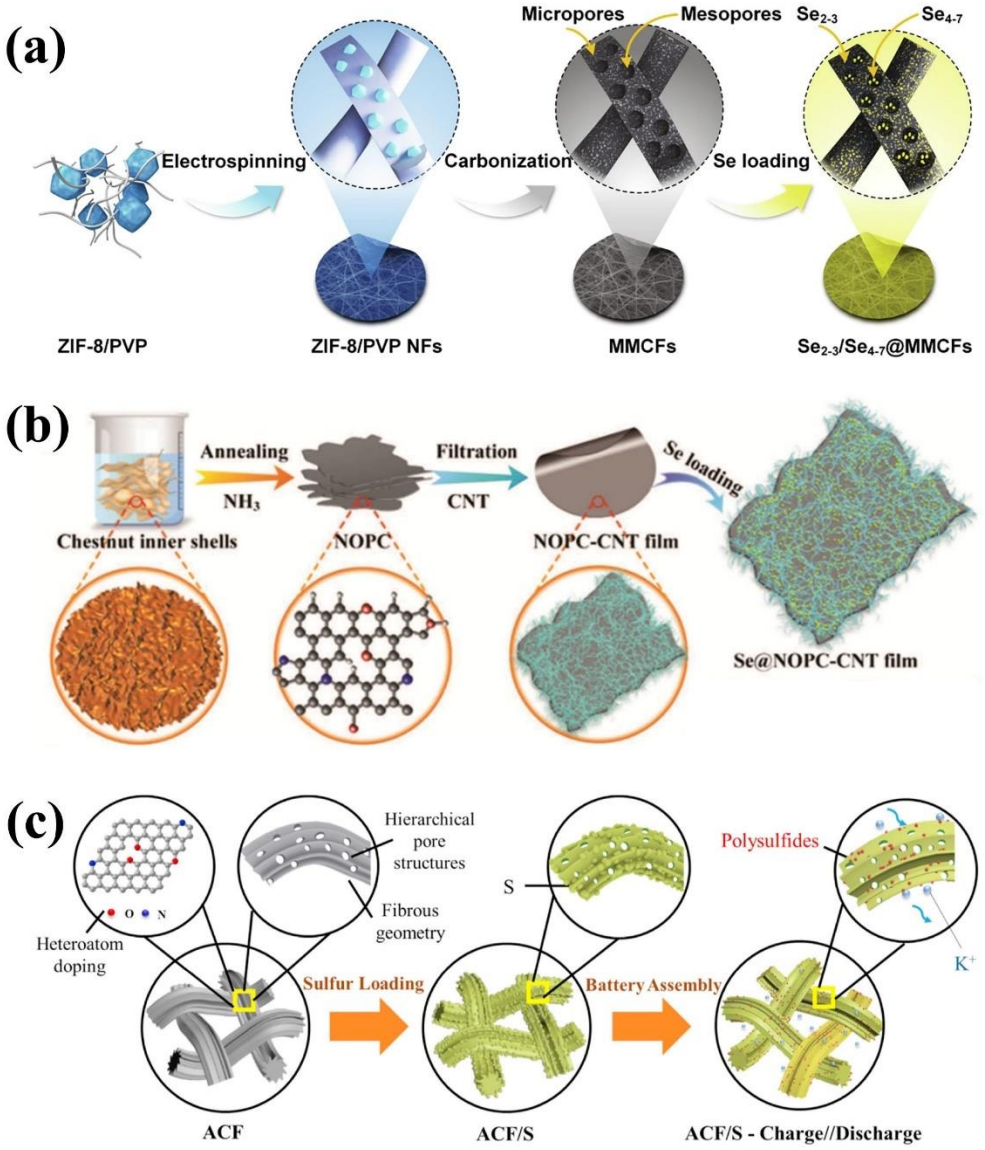

Fig. 8 (a) Formation mechanism of the MMCFs filled with Se molecules.[111] (Reprinted with permission, Copyright 2021, Elsevier). (b) Synthesis procedure of the Se@NOPC-CNT film electrode.[109] (Reprinted with permission, Copyright 2018, Wiley). (c) Synthesis procedure of the ACF@S electrode.[48] (Reprinted with permission, Copyright 2020, Elsevier).

Table 4 Recent progress on electrochemical properties of carbon-based electrodes for flexible K-S/Se batteries.

Materials	Electrolytes	Voltage range	Cycling performance	Rate capability	Device type
Activated carbon fiber @S[48]	3.0 M KFSI DME	1.2–3.0 V	157 mA h g^{-1}@0.05 A g^{-1}/250 cycles		Coin cell
CNT/S[112]	3.0 M KFSI DME	1.2–3.0 V	135 mA h g^{-1}@0.05 A g^{-1}/200 cycles	94 mA h g^{-1}@0.5 A g^{-1}	Coin cell
Se@N, O dual-doped porous carbon nanosheet-CNT[109]	0.7 M KPF_6 EC/DEC (1:1)	0.5–3.0 V	544 mA h g^{-1}@0.1 A g^{-1}/150 cycles 335 mA h g^{-1}@0.8 A g^{-1}/700 cycles	273 mA h g^{-1}@5.0 A g^{-1}	Coin cell
Small-molecule Se@peapod-like N-doped CNFs[113]	0.7 M KPF_6 EC/DEC (1:1)	0.5–3.0 V	635 mA h g^{-1}@0.05 A g^{-1}/50 cycles 367 mA h g^{-1}@0.5 A g^{-1}/1670 cycles	209 mA h g^{-1}@2.0 A g^{-1}	Coin cell
CNTs/CMK-3/Se[114]	5.0 M KTFSI DEGDME	1.2–3.0 V	209 mA h g^{-1}@0.1 C/160 cycles 252 mA h g^{-1}@0.5 C/350 cycles		Coin cell
Se_{2-3}/Se_{4-7}@N/O co-doped CNFs[111]	0.7 M KPF_6 EC/DEC (1:1)	0.5–3.0 V	550 mA h g^{-1}@0.05 A g^{-1}/50 cycles 393 mA h g^{-1}@1.0 A g^{-1}/2000 cycles	256 mA h g^{-1}@5.0 A g^{-1}	Coin cell
SeS_2@nitrogen-doped CNFs[115]	0.7 M KPF_6 EC/DEC (1:1)	0.5–2.8 V	703 mA h g^{-1}@0.05 A g^{-1}/150 cycles 417 mA h g^{-1}@0.5 A g^{-1}/1000 cycles	372 mA h g^{-1}@2.0 A g^{-1}	Coin cell

4. Conclusions and perspectives

In this review, we systematically introduce the recent research advance in carbon materials for flexible electrochemical potassium storage devices including PIBs, PIHCs, and K-S/Se batteries. The common preparation methods of carbon-based flexible electrodes have been presented. The obtained electrochemical performance, voltage windows, and electrolytes are collected, as presented in **Tables 2–4**. Carbon materials have many excellent properties, such as low weight, non-toxicity, and abundance, which make them competitive in flexible electrodes. They can be used as active materials directly and the substrate of composites. When used as active materials, their material properties and electrochemical performance are largely influenced by heteroatom doing, graphitization degree, morphologies, *etc*. As substrate materials, they are normally incorporated with active materials that possess a high theoretical specific capacity, such as alloying materials, metal chalcogenides/phosphides, and organic materials. Herein, it should be mentioned that different carbon materials possess their advantages and shortcomings in terms of electrical conductivity, cost, flexibility, mechanical strength, *etc*. Therefore, in such an application-oriented research field, it is necessary to comprehensively consider and balance various factors during research progress. So far, although the related study has achieved encouraging results as described above, there are still many challenges to be further addressed and substantial room for improvement. Based on the recent advances, five possible research directions in this realm are proposed in the following parts.

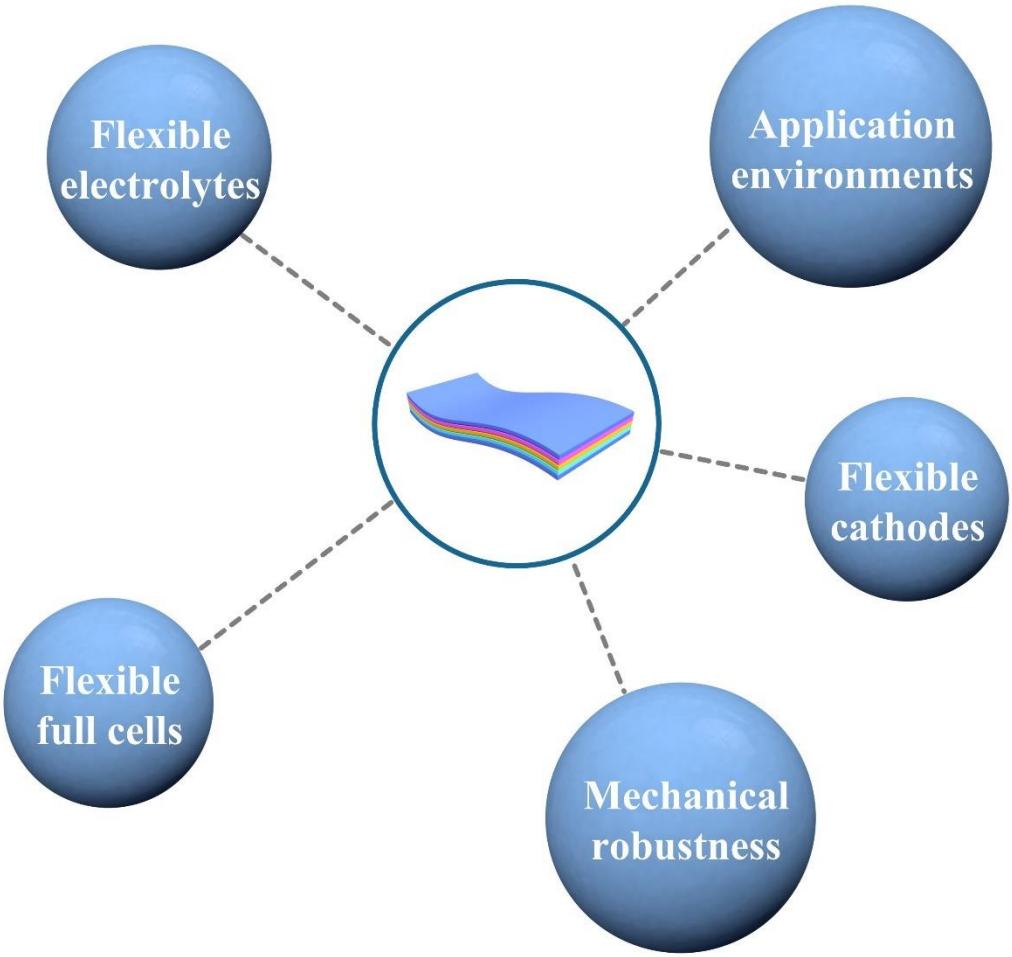

Fig. 9 Possible future directions of K-based flexible EESDs.

(1) Mechanical robustness of flexible electrodes. Previous works mainly focus on simply exhibiting the bendability and elasticity of flexible electrodes or the flexibility of full cells. However, according to different practical application environments, flexible EESDs will face various working modes and will be twisted, folded, distorted, and bent. In this case, flexible electrodes are at risk of crack or even fracture, which directly affects the lifespan, stability, and safety of flexible cells. In addition, the flexibility of flexible electrodes after electrochemical cycling tests has not received enough attention. Therefore, it should be examined the intrinsic mechanical robustness after flexibility testing and the integrity after electrochemical testing. Moreover, relevant evaluation criteria have not been established, and thus, it is highly necessary to set standards to quantify the mechanical robustness of flexible electrodes.

(2) Cathodes used for flexible PIBs. Until now, the report on cathodes for flexible PIBs is quite

rare. For one thing, developed cathode materials are limited; for another thing, these cathode materials are typically ternary or even multi-elemental, which are difficult to directly grow on most flexible carbon substrates. To realize practical application, it is necessary to develop high-performance flexible cathodes to match with flexible anodes for assembling flexible full cells. Prussian blue analogues (PBAs) are a kind of most studied cathode materials due to their superior structures and electrochemical properties. They can be easily loaded on the surface of various carbon materials by hydrothermal, coprecipitation, electrodeposition, *etc*. Layered transition metal oxides and polyanionic compounds are other two popular cathode materials with high operating potentials. Among them, those possessing high-temperature stability may be potential candidates. Firstly, they are embedded into nanofibers by electrospinning to form a composite film. Afterward, the film transfers into a layered transition metal oxide or polyanionic compound/CNF composite flexible electrode.

(3) Flexible electrolytes. Liquid electrolytes are the most used electrolytes in EESDs, but their drawbacks of flammability, toxicity, volatility, fluidity, and potential risk of leakage restrict their safe application. To avoid these issues, solid-state electrolytes have attracted extensive attention. Meanwhile, they have good thermal and electrochemical stability at wide voltage ranges and appropriate mechanical strength to resist metal dendrite growth. Gel polymer electrolytes, as a solid-state electrolyte, composing of a conventional liquid electrolyte and a polymer matrix, not only possess the advantage of solid-state electrolytes, but also inherit the flexibility of gel polymer matrix. They are conducive to developing flexible K-based EESDs. Although the research on K-based gel polymer electrolytes is in its infancy, the advanced experience achieved in the field of LIBs may provide a guiding reference.

(4) Flexible full cells. The electrochemical performance evaluation of most flexible electrodes was carried out in coin cells in terms of half cells, as introduced in Section 3 and shown in **Tables 2–4**. This is far from enough because the electrochemical performance of electrode materials in full cells is more valuable for practical application. Normally, the key electrochemical parameters in half and full cells show significant differences. In full cells, researchers cannot only focus on the electrochemical performance of electrode materials; the choice of coupling electrodes, the ratio of cathodes and anodes, the compatibility of

electrolytes, the voltage window of full cells, *etc*. should also be comprehensively considered. As for flexible K-based full cells, designing and fabricating processes are more complex. For example, flexible substrates are essential, whereas, their contribution to the electrochemical performance is limited or even negative. In addition, attention should also concentrate on the selection and optimization of cell components, such as packaging materials, which directly affect the energy density of flexible full cells.

(5) Application environments. The flexibility of flexible K-based EESDs largely expands their application fields, making their working environments changeable. In this case, special consideration should be given to their electrochemical performance, safety, and durability. For instance, flexible K-based EESDs as the power of flexible electronics face environmental temperatures and environmental chemistry changing frequently. This places greater requirements on flexible K-based EESDs. Therefore, the electrochemical properties of electrode materials and electrolytes at wide temperature ranges and the chemical resistance of packaging materials should be investigated when designing flexible K-based EESDs.

All in all, although there are still many problems and challenges, the excellent material, physical, and chemical properties of carbon materials and the achieved encouraging results in flexible K-based EESDs endow them a bright future in such an emerging field.

Abbreviations

Abbreviation	**Full name**
SEM	Scanning electron microscopy
TEM	Transmission electron microscopy
EC	Ethylene carbonate
DEC	Diethyl carbonate
DME	Dimethoxyethane
DMC	Dimethyl carbonate
DEGDME	Diethylene glycol dimethyl ether
DGM	Diglyme

TEP	Triethyl phosphate
KPF_6	Potassium hexafluorophosphate
KFSI	Potassium bis(fluorosulfonyl)imide
KTFSI	Potassium bis(trifluoromethylsulfonyl)imide
LED	Light-emitting diode

Acknowledgements

The authors acknowledge the support by the Key R&D project of Liaoning Province of China (No. 2020JH2/10300079), the "Liaoning BaiQianWan Talents Program" (No. 2018921006), the Liaoning Revitalization Talents Program (No. XLYC1908034), the Engineering and Physical Sciences Research Council (EP/V000152/1, EP/X000087/1), the Leverhulme Trust (RPG-2021-138), and the Royal Society (RGS\R2\212324, SIF\R2\212002), and Shenyang University of Technology. For the purpose of open access, the author has applied a Creative Commons Attribution (CC BY) licence to any Author Accepted Manuscript version arising. The authors thank Dr. Chenglin Zhang (Jiangsu University) for his helpful discussions.

References

1. Jagadale A., Zhou X., Xiong R., et al. Lithium ion capacitors (LICs): Development of the materials [J]. Energy Storage Materials, 2019, 19: 314-329.

2. Boaretto N., Garbayo I., Valiyaveettil-SobhanRaj S., et al. Lithium solid-state batteries: State-of-the-art and challenges for materials, interfaces and processing [J]. Journal of Power Sources, 2021, 502: 229919.

3. Qi F., Sun Z., Fan X., et al. Tunable interaction between metal-organic frameworks and electroactive components in lithium–sulfur batteries: Status and perspectives [J]. Advanced Energy Materials, 2021, 11(20): 2100387.

4. Eftekhari A. The rise of lithium–selenium batteries [J]. Sustainable Energy & Fuels, 2017, 1(1): 14-29.

5. Yabuuchi N., Kubota K., Dahbi M., et al. Research development on sodium-ion batteries [J].

Chemical Reviews, 2014, 114(23): 11636-11682.

6. Yang S., Zhang F., Ding H., et al. Lithium metal extraction from seawater [J]. Joule, 2018, 2(9): 1648-1651.

7. Li T., Zhao H., Li C.-x., et al. Recent progress and prospects in anode materials for potassium-ion capacitors [J]. New Carbon Materials, 2021, 36(2): 253-277.

8. Vijaya Kumar Saroja A. P., Xu Y. Carbon materials for Na-S and K-S batteries [J]. Matter, 2022, 5(3): 808-836.

9. Zhou J., Liu Y., Zhang S., et al. Metal chalcogenides for potassium storage [J]. InfoMat, 2020, 2(3): 437-465.

10. Wang W., Zhou J., Wang Z., et al. Short-range order in mesoporous carbon boosts potassium-ion battery performance [J]. Advanced Energy Materials, 2018, 8(5): 1701648.

11. Hosaka T., Kubota K., Hameed A. S., et al. Research development on K-ion batteries [J]. Chemical Reviews, 2020, 120(14): 6358-6466.

12. Kubota K., Dahbi M., Hosaka T., et al. Towards K-ion and Na-ion batteries as "beyond Li-ion" [J]. The Chemical Record, 2018, 18(4): 459-479.

13. Qiu W., Xiao H., Li Y., et al. Nitrogen and phosphorus codoped vertical graphene/carbon cloth as a binder-free anode for flexible advanced potassium ion full batteries [J]. Small, 2019, 15(23): 1901285.

14. Wang L., Bao J., Liu Q., et al. Concentrated electrolytes unlock the full energy potential of potassium-sulfur battery chemistry [J]. Energy Storage Materials, 2019, 18: 470-475.

15. Zhang T., Mao Z., Shi X., et al. Tissue-derived carbon microbelt paper: A high-initial-coulombic-efficiency and low-discharge-platform K^+-storage anode for 4.5 V hybrid capacitors [J]. Energy & Environmental Science, 2022, 15(1): 158-168.

16. Wu Y., Zhang C., Zhao H., et al. Recent advances in ferromagnetic metal sulfides and selenides as anodes for sodium- and potassium-ion batteries [J]. Journal of Materials Chemistry A, 2021, 9(15): 9506-9534.

17. Yang G., Wu Y., Fu Q., et al. Nanostructured metal selenides as anodes for potassium-ion batteries [J]. Sustainable Energy & Fuels, 2022, 6(9): 2087-2112.

18. Zhou G., Li F., Cheng H.-M. Progress in flexible lithium batteries and future prospects [J]. Energy & Environmental Science, 2014, 7(4): 1307-1338.

19. Li H., Zhang X., Zhao Z., et al. Flexible sodium-ion based energy storage devices: Recent progress and challenges [J]. Energy Storage Materials, 2020, 26:83-104.

20. Wang D.-K., Zhang J.-K., Dong Y., et al. Progress on graphitic carbon materials for potassium-based energy storage [J]. New Carbon Materials, 2021, 36(3): 435-448.

21. Li X., Wang X.-y., Sun J. Recent progress in the carbon-based frameworks for high specific capacity anodes/cathode in lithium/sodium ion batteries [J]. New Carbon Materials, 2021, 36(1): 106-116.

22. Wen L., Li F., Cheng H. M. Carbon nanotubes and graphene for flexible electrochemical energy storage: From materials to devices [J]. Advanced Materials, 2016, 28(22): 4306-4337.

23. Peng S., Wang L., Zhu Z., et al. Electrochemical performance of reduced graphene oxide/carbon nanotube hybrid papers as binder-free anodes for potassium-ion batteries [J]. Journal of Physics and Chemistry of Solids, 2020, 138: 109296.

24. Xie X., Zhao M.-Q., Anasori B., et al. Porous heterostructured mxene/carbon nanotube composite paper with high volumetric capacity for sodium-based energy storage devices [J]. Nano Energy, 2016, 26: 513-523.

25. Li W., Yang Z., Jiang Y., et al. Crystalline red phosphorus incorporated with porous carbon nanofibers as flexible electrode for high performance lithium-ion batteries [J]. Carbon, 2014, 78: 455-462.

26. Li D., Dai L., Ren X., et al. Foldable potassium-ion batteries enabled by free-standing and flexible SnS_2@C nanofibers [J]. Energy & Environmental Science, 2021, 14(1): 424-436.

27. Zhou C., Fan S., Hu M., et al. High areal specific capacity of $Ni_3V_2O_8$/carbon cloth hierarchical structures as flexible anodes for sodium-ion batteries [J]. Journal of Materials Chemistry A, 2017, 5(30): 15517-15524.

28. Long B., Zhang J., Luo L., et al. High pseudocapacitance boosts the performance of monolithic porous carbon cloth/closely packed TiO_2 nanodots as an anode of an all-flexible sodium-ion battery [J]. Journal of Materials Chemistry A, 2019, 7(6): 2626-2635.

29. Chang S., Pu J., Wang J., et al. Electrochemical fabrication of monolithic electrodes with core/shell sandwiched transition metal oxide/oxyhydroxide for high-performance energy storage [J]. ACS Applied Materials & Interfaces, 2016, 8(39): 25888-25895.

30. Zhang H., Ning H., Busbee J., et al. Electroplating lithium transition metal oxides [J]. Science

Advances, 2017, 3(5): e1602427.

31. Ahmad S., Copic D., George C., et al. Hierarchical assemblies of carbon nanotubes for ultraflexible Li-ion batteries [J]. Advanced Materials, 2016, 28(31): 6705-6710.

32. Pan Z., Ren J., Guan G., et al. Synthesizing nitrogen-doped core-sheath carbon nanotube films for flexible lithium ion batteries [J]. Advanced Energy Materials, 2016, 6(11): 1600271.

33. Xiao X., Li T., Peng Z., et al. Freestanding functionalized carbon nanotube-based electrode for solid-state asymmetric supercapacitors [J]. Nano Energy, 2014, 6: 1-9.

34. Xiao X., Peng X., Jin H., et al. Freestanding mesoporous VN/CNT hybrid electrodes for flexible all-solid-state supercapacitors [J]. Advanced Materials, 2013, 25(36): 5091-5097.

35. Zeng C., Xie F., Yang X., et al. Ultrathin titanate nanosheets/graphene films derived from confined transformation for excellent Na/K ion storage [J]. Angewandte Chemie International Edition, 2018, 57(28): 8540-8544.

36. Inagaki M., Yang Y., Kang F. Carbon nanofibers prepared via electrospinning [J]. Advanced Materials, 2012, 24(19): 2547-2566.

37. Tian Z., Chui N., Lian R., et al. Dual anionic vacancies on carbon nanofiber threaded mosse arrays: A free-standing anode for high-performance potassium-ion storage [J]. Energy Storage Materials, 2020, 27: 591-598.

38. Qiu H., Zhao L., Asif M., et al. SnO_2 nanoparticles anchored on carbon foam as a freestanding anode for high performance potassium-ion batteries [J]. Energy & Environmental Science, 2020, 13(2): 571-578.

39. Atangana Etogo C., Huang H., Hong H., et al. Metal-organic-frameworks-engaged formation of $Co_{0.85}Se$@C nanoboxes embedded in carbon nanofibers film for enhanced potassium-ion storage [J]. Energy Storage Materials, 2020, 24: 167-176.

40. Suo G., Zhang J., Li D., et al. Flexible n doped carbon/bubble-like MoS_2 core/sheath framework: Buffering volume expansion for potassium ion batteries [J]. Journal of Colloid and Interface Science, 2020, 566: 427-433.

41. Gao M. R., Xu Y. F., Jiang J., et al. Nanostructured metal chalcogenides: Synthesis, modification, and applications in energy conversion and storage devices [J]. Chemical Society Reviews, 2013, 42(7): 2986-3017.

42. Pu J., Shen Z., Zhong C., et al. Electrodeposition technologies for Li-based batteries: New frontiers of energy storage [J]. Advanced Materials, 2020, 32(27): 1903808.

43. Yu Q., Jiang B., Hu J., et al. Metallic octahedral $CoSe_2$ threaded by n-doped carbon nanotubes: A flexible framework for high-performance potassium-ion batteries [J]. Advanced Science, 2018, 5(10): 1800782.

44. Ren W., Wang C., Lu L., et al. SnO_2@Si core–shell nanowire arrays on carbon cloth as a flexible anode for Li ion batteries [J]. Journal of Materials Chemistry A, 2013, 1(43): 13433-13438.

45. Suo G., Zhang J., Li D., et al. N-doped carbon/ultrathin 2D metallic cobalt selenide core/sheath flexible framework bridged by chemical bonds for high-performance potassium storage [J]. Chemical Engineering Journal, 2020, 388: 124396.

46. Hwang J. Y., El-Kady M. F., Wang Y., et al. Direct preparation and processing of graphene/RuO_2 nanocomposite electrodes for high-performance capacitive energy storage [J]. Nano Energy, 2015, 18: 57-70.

47. Wan F., Huang S., Cao H., et al. Freestanding potassium vanadate/carbon nanotube films for ultralong-life aqueous zinc-ion batteries [J]. ACS Nano, 2020, 14(6): 6752-6760.

48. Yuan X., Zhu B., Feng J., et al. Free-standing, flexible and stable potassium–sulfur battery enabled by controllable porous carbon cloth [J]. Journal of Power Sources, 2020, 480: 228874.

49. Zhao X., Xiong P., Meng J., et al. High rate and long cycle life porous carbon nanofiber paper anodes for potassium-ion batteries [J]. Journal of Materials Chemistry A, 2017, 5(36): 19237-19244.

50. Xu Y., Yuan T., Zhao Y., et al. Constructing multichannel carbon fibers as freestanding anodes for potassium-ion battery with high capacity and long cycle life [J]. Advanced Materials Interfaces, 2019, 7(3): 1901829.

51. Yang W., Zhou J., Wang S., et al. Freestanding film made by necklace-like N-doped hollow carbon with hierarchical pores for high-performance potassium-ion storage [J]. Energy & Environmental Science, 2019, 12(5): 1605-1612.

52. Wu Y., Xu R., Wang Z., et al. Carbon-free crystal-like $Fe_{1-x}S$ as an anode for potassium-ion batteries [J]. ACS Applied Materials & Interfaces, 2021, 13(46): 55218-55226.

53. Wu Y., Xu R., Wang Z., et al. Carbon-free crystal-like fe1-xs as an anode for potassium-ion batteries [J]. ACS Appl Mater Interfaces, 2021, 13(46): 55218-55226.

54. Lao M., Zhang Y., Luo W., et al. Alloy-based anode materials toward advanced sodium-ion batteries [J]. Advanced Materials, 2017, 29(48): 1700622.

55. Song K., Liu C., Mi L., et al. Recent progress on the alloy-based anode for sodium-ion batteries and potassium-ion batteries [J]. Small, 2021, 17(9): 1903194.

56. Ge X., Liu S., Qiao M., et al. Enabling superior electrochemical properties for highly efficient potassium storage by impregnating ultrafine Sb nanocrystals within nanochannel-containing carbon nanofibers [J]. Angewandte Chemie International Edition, 2019, 58(41): 14578-14583.

57. Jin T., Li H., Li Y., et al. Intercalation pseudocapacitance in flexible and self-standing V_2O_3 porous nanofibers for high-rate and ultra-stable K ion storage [J]. Nano Energy, 2018, 50: 462-467.

58. Dai J., Su D., Yang J., et al. A flexible $Mn_{0.5}Ti_2(PO_4)_3$/C nanofiber film with superior cycling stability for potassium-ion batteries [J]. Nanoscale, 2021, 13(47): 19956-19965.

59. Yi Z., Liu Y., Li Y., et al. Flexible membrane consisting of MoP ultrafine nanoparticles highly distributed inside N and P codoped carbon nanofibers as high-performance anode for potassium-ion batteries [J]. Small, 2020, 16(2): 1905301.

60. Sehrawat P., Julien C., Islam S. S. Carbon nanotubes in Li-ion batteries: A review [J]. Materials Science and Engineering: B, 2016, 213: 12-40.

61. Li X., Zhuang C., Xu J., et al. Rational construction of $K_{0.5}V_2O_5$ nanobelts/CNTs flexible cathode for multi-functional potassium-ion batteries [J]. Nanoscale, 2021, 13(17): 8199-8209.

62. Bolotin K. I., Sikes K. J., Jiang Z., et al. Ultrahigh electron mobility in suspended graphene [J]. Solid State Communications, 2008, 146(9-10): 351-355.

63. Ojha R. P., Lemieux P. A., Dixon P. K., et al. Statistical mechanics of a gas-fluidized particle [J]. Nature, 2004, 427(6974): 521-523.

64. Balandin A. A., Ghosh S., Bao W., et al. Superior thermal conductivity of single-layer graphene [J]. Nano Letters, 2008, 8(3): 902-907.

65. Lv W., Li Z., Deng Y., et al. Graphene-based materials for electrochemical energy storage devices: Opportunities and challenges [J]. Energy Storage Materials, 2016, 2: 107-138.

66. Chen K., Song S., Liu F., et al. Structural design of graphene for use in electrochemical energy storage devices [J]. Chemical Society Reviews, 2015, 44(17): 6230-6257.

67. Zhang Z., Wu C., Chen Z., et al. Spatially confined synthesis of a flexible and hierarchically porous

three-dimensional graphene/FeP hollow nanosphere composite anode for highly efficient and ultrastable potassium ion storage [J]. Journal of Materials Chemistry A, 2020, 8(6): 3369-3378.

68. Zeng L., Liu M., Li P., et al. A high-volumetric-capacity bismuth nanosheet/graphene electrode for potassium ion batteries [J]. Science China Materials, 2020, 63(10): 1920-1928.

69. Zeng S., Chen X., Xu R., et al. Boosting the potassium storage performance of carbon anode via integration of adsorption-intercalation hybrid mechanisms [J]. Nano Energy, 2020, 73: 104807.

70. Zhang H., Huang Y., Ming H., et al. Recent advances in nanostructured carbon for sodium-ion batteries [J]. Journal of Materials Chemistry A, 2020, 8(4): 1604-1630.

71. Chen Y., Lu Z., Zhou L., et al. In situ formation of hollow graphitic carbon nanospheres in electrospun amorphous carbon nanofibers for high-performance Li-based batteries [J]. Nanoscale, 2012, 4(21): 6800-6805.

72. Chen D., Huang Z., Sun S., et al. A flexible multi-channel hollow CNT/carbon nanofiber composites with S/N co-doping for sodium/potassium ion energy storage [J]. ACS Applied Materials & Interfaces, 2021, 13(37): 44369-44378.

73. Niu P., Wang P., Xu Y., et al. Tuning the electronic conductivity of porous nitrogen-doped carbon nanofibers with graphene for high-performance potassium-ion storage [J]. Inorganic Chemistry Frontiers, 2021, 8(16): 3926-3933.

74. Adams R. A., Syu J.-M., Zhao Y., et al. Binder-free N- and O-rich carbon nanofiber anodes for long cycle life K-ion batteries [J]. ACS Applied Materials & Interfaces, 2017, 9(21): 17872-17881.

75. Zhang M., Shoaib M., Fei H., et al. Hierarchically porous n-doped carbon fibers as a free-standing anode for high-capacity potassium-based dual-ion battery [J]. Advanced Energy Materials, 2019, 9(37): 1901663.

76. Sun H., Zhu W., Yuan F., et al. Hierarchical porous carbon nanofibers with enhanced capacitive behavior as a flexible self-supporting anode for boosting potassium storage [J]. Journal of Power Sources, 2022, 523: 231043.

77. Cao K., Liu H., Jia Y., et al. Flexible antimony@carbon integrated anode for high-performance potassium-ion battery [J]. Advanced Materials Technologies, 2020, 5(6): 2000199.

78. Mao M., Cui C., Wu M., et al. Flexible ReS_2 nanosheets/N-doped carbon nanofibers-based paper as a universal anode for alkali (Li, Na, K) ion battery [J]. Nano Energy, 2018, 45: 346-352.

79. Zhu X., Gao J., Li J., et al. Self-supporting N-rich Cu_2Se/C nanowires for highly reversible, long-life potassium-ion storage [J]. Sustainable Energy & Fuels, 2020, 4(5): 2453-2461.

80. Sun H., Su Y., Yuan F., et al. Fe_2P nanoparticles-doped carbon nanofibers with enhanced electrons transfer capability as a self-supporting anode for potassium-ion battery [J]. Electrochimica Acta, 2022, 404: 139759.

81. Li X., Sun N., Tian X., et al. Electrospun coal liquefaction residues/polyacrylonitrile composite carbon nanofiber nonwoven fabrics as high-performance electrodes for lithium/potassium batteries [J]. Energy & Fuels, 2020, 34(2): 2445-2451.

82. Yao G., Lin M., Yang J., et al. Stabilizing V_2O_3 in carbon nanofiber flexible films for ultrastable potassium storage [J]. Inorganic Chemistry Frontiers, 2022, 9(7): 1434-1445.

83. Zhao Y., Ruan J., Luo S., et al. Rational construction of a binder-free and universal electrode for stable and fast alkali-ion storage [J]. ACS Applied Materials & Interfaces, 2019, 11(43): 40006-40013.

84. Zhang E., Jia X., Wang B., et al. Carbon dots@rGO paper as freestanding and flexible potassium-ion batteries anode [J]. Advanced Science, 2020, 7(15): 2000470.

85. Yang Z., Li W., Zhang G., et al. Constructing Sb–O–C bond to improve the alloying reaction reversibility of free-standing Sb_2Se_3 nanorods for potassium-ion batteries [J]. Nano Energy, 2022, 93, 106764.

86. Shen C., Yuan K., Tian T., et al. Flexible sub-micro carbon fiber@CNTs as anodes for potassium-ion batteries [J]. ACS Applied Materials & Interfaces, 2019, 11(5): 5015-5021.

87. Huang Z., Ding S., Li P., et al. Flexible Sb-graphene-carbon nanofibers as binder-free anodes for potassium-ion batteries with enhanced properties [J]. Nanotechnology, 2021, 32(2): 025401.

88. Han J., Zhu K., Liu P., et al. N-doped CoSb@C nanofibers as a self-supporting anode for high-performance K-ion and Na-ion batteries [J]. Journal of Materials Chemistry A, 2019, 7(44): 25268-25273.

89. Li P., Wang W., Gong S., et al. Hydrogenated $Na_2Ti_3O_7$ epitaxially grown on flexible N-doped carbon sponge for potassium-ion batteries [J]. ACS Applied Materials & Interfaces, 2018, 10(44): 37974-37980.

90. Zeng S., Zhou X., Wang B., et al. Freestanding CNT-modified graphitic carbon foam as a flexible anode for potassium ion batteries [J]. Journal of Materials Chemistry A, 2019, 7(26): 15774-15781.

91. Cao B., Liu H., Zhang P., et al. Flexible mxene framework as a fast electron/potassium-ion dual-function conductor boosting stable potassium storage in graphite electrodes [J]. Advanced Functional Materials, 2021, 31(32): 2102126.

92. Wang D., Du G., Han D., et al. Porous flexible nitrogen-rich carbon membranes derived from chitosan as free-standing anodes for potassium-ion and sodium-ion batteries [J]. Carbon, 2021, 181: 1-8.

93. Sun Y., Zhang Y., Xing Z., et al. A hollow neuronal carbon skeleton with ultrahigh pyridinic n content as a self-supporting potassium-ion battery anode [J]. Sustainable Energy & Fuels, 2020, 4(3): 1216-1224.

94. Yang Y., Wang L., Zeng S., et al. FeP coated in nitrogen/phosphorus co-doped carbon shell nanorods arrays as high-rate capable flexible anode for K-ion half/full batteries [J]. Journal of Colloid and Interface Science, 2022, 624, 670-679.

95. Li N., Jiang Z., Wu X., et al. An interface-free integrative graphitic carbon network film with defective and S/O-codoped hollow units for voltage-stable, ultra-fast and long-life potassium ion storage [J]. Chemical Engineering Journal, 2022, 431, 133736.

96. Zhang Y., Jiang J., An Y., et al. Sodium-ion capacitors: Materials, mechanism, and challenges [J]. ChemSusChem, 2020, 13(10): 2522-2539.

97. Hu X., Zhong G., Li J., et al. Hierarchical porous carbon nanofibers for compatible anode and cathode of potassium-ion hybrid capacitor [J]. Energy & Environmental Science, 2020, 13(8): 2431-2440.

98. Yan D., Han B., Wang Z., et al. Engineered phase of nickel sulfides inside hairy hollow fibers towards high-performance anodes for flexible potassium ion hybrid capacitors [J]. Journal of Materials Chemistry A, 2022, 10(10): 5569-5579.

99. Chen M., Wang L., Sheng X., et al. An ultrastable nonaqueous potassium-ion hybrid capacitor [J]. Advanced Functional Materials, 2020, 30(40): 2004247.

100. Jia M., Tian S., Yin G., et al. Hollow MoS_2 spheres confined in carbon fibers for ultralong-life potassium storage [J]. ACS Applied Energy Materials, 2022, 5(3): 3605-3614.

101. Luo Z., Zhang Q., Xie W., et al. B, F co-doping flexible carbon nanofibers as a fast and stable anode for potassium-ion hybrid capacitor [J]. Journal of Alloys and Compounds, 2022, 914: 165285.

102. Xiong Q., He H., Zhang M. Design of flexible films based on kinked carbon nanofibers for high rate and stable potassium-ion storage [J]. Nano-Micro Letters, 2022, 14(1): 1-17.

103. Wang D., Wang P., Lu B., et al. Porous carbon tubes constructing freestanding flexible electrodes for symmetric potassium-ion hybrid capacitors [J]. ACS Applied Energy Materials, 2021, 4(12): 13593-13604.

104. Li X., Li D., Cai J., et al. Kinetically boosted potassium ion storage capability of 1D $K_2Ti_6O_{13}$ nanobelts by 3D porous carbon framework for fiber-shaped potassium ion capacitors [J]. Journal of Power Sources, 2022, 533: 231419.

105. Yan D., Xie M., Shao Y., et al. Fast and durable anodes for sodium-/potassium-ion hybrid capacitors: Tailoring self-adaptive nanocages inside hybrid fibers with high alignment [J]. Journal of Materials Chemistry A, 2021, 9(24): 13986-13995.

106. Wei S., Deng X., Kundu M., et al. Bead-like coal-derived carbon anodes for high performance potassium-ion hybrid capacitors [J]. ChemElectroChem, 2022, 9(9), e202101715.

107. Ma R., Fan L., Wang J., et al. Confined and covalent sulfur for stable room temperature potassium-sulfur battery [J]. Electrochimica Acta, 2019, 293: 191-198.

108. Huang X. L., Guo Z., Dou S. X., et al. Rechargeable potassium–selenium batteries [J]. Advanced Functional Materials, 2021, 31(29): 2102326.

109. Yao Y., Chen M., Xu R., et al. CNT interwoven nitrogen and oxygen dual-doped porous carbon nanosheets as free-standing electrodes for high-performance Na-Se and K-Se flexible batteries [J]. Advanced Materials, 2018, 30(49): 1805234.

110. Huang X., Deng J., Qi Y., et al. A highly-effective nitrogen-doped porous carbon sponge electrode for advanced K-Se batteries [J]. Inorganic Chemistry Frontiers, 2020, 7(5): 1182-1189.

111. Li D., Wang L., Cheng X., et al. Manipulating selenium molecular configuration in N/O dual-doped porous carbon for high performance potassium-ion storage [J]. Journal of Energy Chemistry, 2021, 62: 581-589.

112. Yuan X., Zhu B., Feng J., et al. High-performance stable potassium–sulfur batteries enabled by free-standing cnt film-based composite cathodes [J]. Journal of Electronic Materials, 2021, 50(6): 3037-3042.

113. Xu R., Yao Y., Wang H., et al. Unraveling the nature of excellent potassium storage in small-

molecule Se@peapod-like N-doped carbon nanofibers [J]. Advanced Materials, 2020, 32(52): 2003879.
114.Liu Q., Deng W., Pan Y., et al. Approaching the voltage and energy density limits of potassium–selenium battery chemistry in a concentrated ether-based electrolyte [J]. Chemical Science, 2020, 11(23): 6045-6052.
115.Yao Y., Xu R., Chen M., et al. Encapsulation of SeS_2 into nitrogen-doped free-standing carbon nanofiber film enabling long cycle life and high energy density K-SeS_2 battery [J]. ACS Nano, 2019, 13(4): 4695-4704.